(2)

NAVAL POSTGRADUATE SCHOOL

Monterey, California

THESIS

BUBBLE DETECTION USING A DUAL FREQUENCY SOUND FIELD

by

Ernest R. Lineberger, III

December 1988

Thesis Advisor: Anthony A. Atchley

Unclassified
SECURITY CLASSIFICATION OF THIS PAGE

REPORT DOCUMENTATION PAGE

1a REPORT SECURITY CLASSIFICATION Unclassified	1b RESTRICTIVE MARKINGS
2a SECURITY CLASSIFICATION AUTHORITY	3 DISTRIBUTION / AVAILABILITY OF REPORT Approved for public release, distribution is unlimited
2b DECLASSIFICATION / DOWNGRADING SCHEDULE	
4 PERFORMING ORGANIZATION REPORT NUMBER(S)	5 MONITORING ORGANIZATION REPORT NUMBER(S)
6a NAME OF PERFORMING ORGANIZATION Naval Postgraduate School 6b OFFICE SYMBOL (If applicable) 61	7a NAME OF MONITORING ORGANIZATION Naval Postgraduate School
6c ADDRESS (City, State, and ZIP Code) Monterey, CA 93943-5000	7b ADDRESS (City, State, and ZIP Code) Monterey, CA 93943-5000
8a NAME OF FUNDING / SPONSORING ORGANIZATION 8b OFFICE SYMBOL (If applicable)	9 PROCUREMENT INSTRUMENT IDENTIFICATION NUMBER
8c ADDRESS (City, State, and ZIP Code)	10 SOURCE OF FUNDING NUMBERS PROGRAM ELEMENT NO / PROJECT NO / TASK NO / WORK UNIT ACCESSION NO

11 TITLE (Include Security Classification)
BUBBLE DETECTION USING A DUAL FREQUENCY SOUND FIELD

12 PERSONAL AUTHOR(S)
Lineberger, Ernest R.

13a TYPE OF REPORT	13b TIME COVERED	14 DATE OF REPORT (Year, Month, Day)	15 PAGE COUNT
Master's Thesis	FROM ____ TO ____	December 1988	128

16 SUPPLEMENTARY NOTATION The views expressed in this thesis are those of the author and do not reflect the official policy or position of the Department of Defense or the United States Government.

17 COSATI CODES		
FIELD	GROUP	SUB-GROUP

18 SUBJECT TERMS (Continue on reverse if necessary and identify by block number)
Bubble Resonance Frequency, Nonlinear Bubble Dynamics, Bubble Detection, Bubble Size, Dual Frequency, theses, (nsm)

19 ABSTRACT (Continue on reverse if necessary and identify by block number)
The design, testing and analysis of a dual frequency system to detect and determine the resonance frequency (and hence the size) of bubbles ranging from 100 to 7 μm radius is reported. The resonance frequencies were compared to estimates based on the rise time of the bubbles. In general these comparisons agreed to within five percent. Although the system is not ideal for field measurements, it identifies important requirements concerning the size of the sample volume, the frequency and amplitude ranges of the sound fields and signal processing techniques to make an effective system. Bubbles are distinguished from non-gaseous particles by the nature of their nonlinear response to the dual sound field. The system is versatile and can be modified to suit many research purposes.

20 DISTRIBUTION / AVAILABILITY OF ABSTRACT	21 ABSTRACT SECURITY CLASSIFICATION
☒ UNCLASSIFIED/UNLIMITED ☐ SAME AS RPT ☐ DTIC USERS	Unclassified

22a NAME OF RESPONSIBLE INDIVIDUAL	22b TELEPHONE (Include Area Code)	22c OFFICE SYMBOL
Professor Anthony A. Atchley, Code 61Ay	(408) 646-2848	61Ay

DD FORM 1473, 84 MAR 83 APR edition may be used until exhausted
All other editions are obsolete

SECURITY CLASSIFICATION OF THIS PAGE

Approved for Public Release; Distribution is Unlimited

Bubble Detection Using a Dual Frequency Sound Field

by

Ernest R. Lineberger, III
Lieutenant, United States Navy
B. S., University of Southern California, 1980

Submitted in partial fulfillment of the requirements for the degrees of

MASTER OF SCIENCE IN ENGINEERING ACOUSTICS

and

MASTER OF SCIENCE IN SYSTEMS TECHNOLOGY

(Antisubmarine Warfare)

from the

NAVAL POSTGRADUATE SCHOOL
December 1988

Author: _____
Ernest R. Lineberger, III

Approved by: _____
Anthony A. Atchley, Thesis Advisor

_____
Herman Medwin, Second Reader

_____
Anthony A. Atchley, Chairman
Engineering Acoustics Academic Committee

_____
Robert N. Forrest, Chairman
Antisubmarine Warfare Academic Group

_____
Gordon E. Schacher
Dean of Science and Engineering

_____
Harrison Shull
Academic Dean

ABSTRACT

The design, testing and analysis of a dual frequency system to detect and determine the resonance frequency (and hence the size) of bubbles ranging from 100 to 7 μm radius is reported. The resonance frequencies were compared to estimates based on the rise time of the bubbles. In general these comparisons agreed to within five percent. Although the system is not ideal for field measurements, it identifies important requirements concerning the size of the sample volume, the frequency and amplitude ranges of the sound fields and signal processing techinques to make an efective system. Bubbles are distinguished from non-gaseous particles by the nature of their nonlinear response to the dual sound field. The system is versatile and can be modified to suit many research purposes.

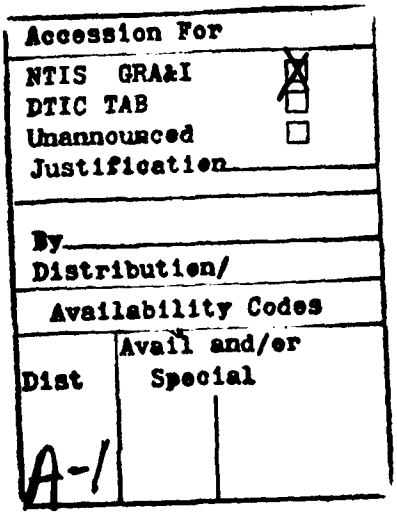

TABLE OF CONTENTS

I. INTRODUCTION

Bubbles in the ocean create a wide variety of effects on sound propagation including absorption and scattering of acoustic energy. In order to develop an accurate model of these effects, it is important to determine the number and size of bubbles in the regions of interest. This thesis reports on an implementation of the dual frequency method to detect bubbles and determine their resonance frequency.

This implementation was conceived with the following goals in mind:

* Detect bubbles with resonance frequencies from 30 kHz to 400 kHz using the dual frequency method published by Newhouse and Shankar [Ref. 1] and investigated by Hampton [Ref. 2].
* Measure the resonance frequency of bubbles as they are detected.
* Distinguish between bubbles and non-gaseous particles.
* Determine the parameters required for a high probability of detection for bubbles in the sample volume.

The dual frequency method is explained in the theory section. Supporting theories regarding bubble resonance, visual determination of bubble size and nonlinear mixing properties of solids are included. The problem approach section details the experimental apparatus and tests. The results of the measurements are then presented and discussed. This thesis concludes with a summary and recommendations for future work in this area.

II. THEORY

The dual frequency method of bubble detection and sizing relies on the nonlinear properties of bubbles undergoing large amplitude oscillations. Theories concerning the characteristics of bubble resonance and nonlinear signal generation by bubbles in a dual frequency sound field are presented to clarify the dual frequency method. Also, because one of the goals of this project is to distinguish between bubbles and solid particles, it is necessary to understand how sound is scattered by solid particles exposed to a dual frequency sound field. A discussion of radiation pressure, streaming and rectified diffusion is included since these mechanisms limit the allowable pressure amplitudes. A section on bubble rise time sizing covers the method used to verify the resonance frequency of certain bubbles by an alternate means.

A. BUBBLE RESONANCE

The fundamental response of a bubble to a perturbation is a purely radial uniform volume pulsation in which the bubble oscillates about its equilibrium radius while maintaining its spherical shape. This approximates a perfect monopole source. Other responses, harmonics, may also occur, but the fundamental is the most efficient radiator of sound and dominates our interest.

The frequency of this fundamental volume pulsation is determined by the stiffness of the gas plus the surface tension and a mass contribution from entrained fluid. Many derivations have been published relating a bubble's equilibrium radius to its resonance frequency. One of the most complete treatments is found in Clay and Medwin [Ref. 3]. The resonance frequencies of air bubbles of given radii at 10 cm depth of fresh water as calculated using Equation 1 [Ref. 3:eq. 6.3.11:p. 197] are given in Table 1. Here, b and β are functions that correct for the adiabatic assumption and surface tension. These two corrections are counteracting and result in very little change to the value calculated by ignoring them. Nonetheless, they were included for accuracy.

$$f_R = \frac{1}{2\pi a}\left[\frac{3\gamma b\beta\, p_A}{\rho_A}\right]^{\frac{1}{2}} \qquad (1)$$

where,

a = bubble radius in cm

γ = ratio of specific heats, C_p/C_v; taken to be 1.402

P_A = ambient pressure on the bubble corrected for depth in dynes/cm^2

ρ_A = ambient density of the fluid surrounding the bubble taken to be 1.03 gm/cm^3

See [Ref. 3] for expressions for b and β.

TABLE 1* RESONANCE FREQUENCY FOR A GIVEN BUBBLE RADIUS INCLUDING CORRECTIONS FOR DEPTH (10 CM), SURFACE TENSION AND THERMAL CONDUCTIVITY

Bubble Radius, a (μm)	Resonance Frequency (kHz)
100	31.4
70	44.6
50	62.1
40	77.3
30	102.6
20	152.9
10	303.8
9	337.7
8	380.4
7	435.8
6	510.8
5	618.0

* The data in this table is included in the Easy Reference Table in the Appendix.

Factors directly effecting the resonance frequency include the volume and type of gas, properties of the fluid medium and depth of the bubble. For this experiment the gas was generated by electrolysis. Various gases can be generated by this method depending on the concentration of chemicals, such as salts, in the water and the voltage applied. The gas produced in this experiment was probably hydrogen, H_2. Chlorine, Cl_2 and Oxygen, O_2 are the other possibilities. Since these gases are all diatomic, they share some common properties. The principle property of interest is the ratio of specific heats, which is listed in Table 2 for these gases and air. Also listed is the approximate error induced by using the specific heat ratio for air in each case. Since these errors are small and many bubble properties have been determined and published for air bubbles in water, air was assumed to be the gas in the bubbles for all calculations. This also allows these results to be more quickly related to any fresh water air bubble situation.

TABLE 2 SPECIFIC HEAT RATIOS FOR SOME GASES

GAS	SPECIFIC HEAT RATIO	RESONANCE FREQ. ERROR FROM AIR
Air	1.402	0.00%
H_2	1.41	0.28%
O_2	1.40	0.07%
Cl_2	1.34	2.24%

Other factors which effect the resonance frequency, such as the depth, pressure, radius and fluid density, are all interrelated. Assuming the mass of gas in the bubble stays constant, a depth increase raises the pressure and decreases the bubbles radius. All of these changes contribute to an increase in the resonance frequency. On the other hand a fluid density increase lowers the resonance frequency. A gas with a larger specific heat ratio would have a higher resonance frequency. For this experiment, all resonance frequencies are given for air bubbles at 10 cm depth of fresh water with a surface pressure of one atmosphere.

The response of a bubble to an excitation is most dramatic when the frequency of the excitation is exactly equal to the resonance frequency of the bubble. The bubble's response at resonance is much greater than the response off resonance as shown in Figure 1 [Ref. 3:Figure 6.4.1: p.204].

Due to the large amplitude oscillations of the bubble driven at resonance, the higher order terms in the bubble's equation of motion are not small with respect to the linear terms. These higher order terms are necessary for the dual frequency method to work.

B. DUAL FREQUENCY EXCITATION AND RESPONSE

References 1 and 2 give extensive treatments of the oscillations of a bubble under the influence of two impinging

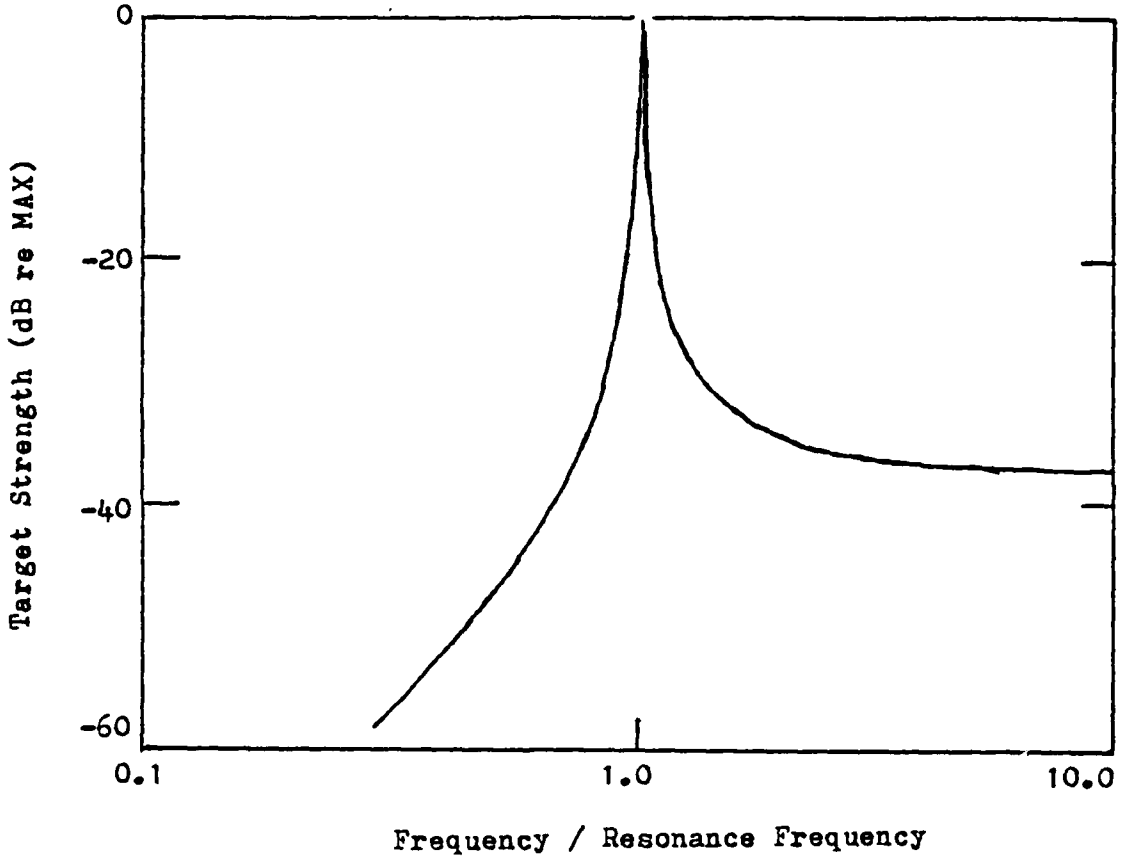

Figure 1 Frequency Response for Single Bubbles

sound fields of different frequencies, f_1 and f_2. f_1 is taken to be a high frequency, much higher than the bubble's resonance frequency, yet with a corresponding wavelength longer than the diameters of the bubbles of interest. f_2 is a lower frequency, at or near the bubble's resonance frequency. As the bubble enters the sound fields, it is excited into large amplitude resonant oscillations by f_2. It is also excited by f_1, although at a much lower amplitude. The result is that the bubble extracts energy from these sound fields and reradiates sound as a monopole source. Because the large amplitude oscillations are nonlinear, the bubble radiates sound at f_1 and f_2, as well as at the sum $(f_1 + f_2)$ and difference $(f_1 - f_2)$ frequencies. All other possible combinations are also radiated, but at much lower amplitudes. This natural frequency mixing is the cornerstone of the dual frequency method.

1. The Resonant Bubble's Response to Dual Frequency Excitation

Isolating our attention to the sum frequency, the pressure radiated by a bubble is given by Equation 2 [Ref. 1].

$$p_+ = \frac{p_1 \, p_2}{\rho \, a \, W_R^2 \, \delta \, r} \qquad (2)$$

where,

ρ = density of fluid

p_1 = acoustic pressure amplitude at frequency f_1 at the location of the bubble

p_2 = acoustic pressure amplitude at frequency f_2 at the location of the bubble

p_+ = acoustic pressure amplitude at the sum frequency $(f_1 + f_2)$ at the location of the receiver

W_R = resonance (angular) frequency of the bubble

δ = damping coefficient

r = distance from bubble to receiver

It has been assumed that f_2 is equal to f_R, the bubble's resonance frequency. The sum frequency pressure amplitude is inversely proportional to the distance, r, from the bubble. The damping coefficient, δ, is claimed to be almost independent of frequency in Reference 1. Values of δ for given bubble sizes at sea level are taken from Reference 3 and listed in Table 3. Using Tables 1 and 3, the density of the fluid and an assumed distance from the bubble to the receiver, the sum frequency pressure amplitude at the receiver can be calculated for the bubble sizes of interest in terms of p_1 and p_2. This information is shown in Table 4.

f_1 performs a task similar to that of the carrier frequency of a radio transmission. Hence, in this thesis f_1

TABLE 3* DAMPING COEFFICIENT FOR SOME BUBBLE SIZES (NUMBERS READ FROM FIGURE 6.3.1, P. 199, REFERENCE 3)

Bubble Radius, a (μm)	δ (Damping Coefficient)
100	0.075
70	0.085
50	0.095
40	0.100
30	0.115
20	0.13
10	0.16
<10	0.16

* The data in this table is included in the Easy Reference Table in the Appendix.

TABLE 4* RATIO OF SUM FREQUENCY PRESSURE AT THE RECEIVER FACE TO THE PRODUCT OF SOUND FIELD PRESSURES p_1 AND p_2 AT THE BUBBLE

Bubble Radius, a (μm)	$\frac{p+}{p_1 p_2}$ (x $10^{+9} Pa^{-1}$)
100	43.2
70	27.0
50	17.4
40	13.4
30	8.79
20	5.25
10	2.16
9	1.94
8	1.72
7	1.50
6	1.28
5	1.05

* The data in this table is included in the Easy Reference Table in the Appendix.

is called the carrier frequency. It can be any convenient frequency high enough with respect to the resonance frequencies of the bubbles of interest that the harmonics of these bubbles are significantly less than the expected difference frequencies. This prevents confusing a harmonic with the difference frequency. The bubbles of interest must have diameters small with respect to the wavelength associated with f_1, so that it oscillates uniformly.

The bubbles of interest to this investigation have radii from 100 down to 7 μm which corresponds to resonance frequencies from approximately 20 to 400 kHz. A reasonable minimum wavelength for these bubbles is 400 μm, which corresponds to a maximum carrier frequency of 3.7 MHz. This ensures the acoustic wavelength is at least four times the largest bubble radius. Assuming harmonics higher than the third or fourth will be insignificant leads to a minimum carrier frequency of about 5 times the highest bubble resonance or 2.0 MHz. The actual value of f_1 used in this experiment was 2.65 MHz which is near the center of this frequency range.

The purpose of f_2 is to excite the bubbles into large amplitude resonant oscillations. For this reason, f_2 is called the excitation frequency. It must encompass the range of resonance frequencies of the bubbles of interest. This means that f_2 must cover the full range from 30 to 400 kHz

continuously. Two schemes for producing f_2 are possible. One as sweeping the frequency repeatedly over the desired range. This method will periodically excite any bubble in the range, but only for a short time. Another option is broadcasting band limited white noise covering the proper frequency range. This more continuously excites any bubble in the range at its resonance frequency. This second method was chosen so that all bubbles will always find their resonance frequency in the f_2 sound field. This method requires more power since it broadcasts over a large bandwidth continuously at moderate amplitude.

Using noise to ensure the resonance frequencies of interest are present also ensures that additional frequencies are present. This does not confound the dual frequency method though, since each bubble naturally responds strongest to its resonance frequency. Due to the large quality factors, the bubbles will vibrate strongly at their resonance frequencies and greatly ignore the sound energy at other nearby frequencies. This will allow the detected sum frequency to pinpoint the resonance frequency, f_R, of the bubble that generated it. $f_R = f_{sum} - f_{carrier}$.

As bubbles get smaller their acoustical cross sections (absorption, scattering and extinction) become smaller. To keep smaller bubbles excited strongly enough to produce observable dual frequency mixing, coloring the noise sound field is necessary. A ramp function that causes more sound

energy at the higher frequencies alleviates this problem somewhat.

A relatively large bubble responds strongly at its resonance frequency and also scatters higher frequencies. The scattered amplitude can be higher than the amplitude due to a bubble resonant at the higher frequency due to the larger bubble's large scattering cross section. This leads to an ambiguity for other methods as shown by curve b of Figure 2 [Ref. 1]. For a uniform distribution of bubble radii in the mixture, a high bubble resonance frequency may be detected at high amplitude due to either, (1) a resonant bubble or (2) a much larger scattering bubble. Bubble scattering detection techniques looking for the bubble's resonance frequency directly cannot be sure which of these mechanisms is causing the signal without more information. Reference 3 discusses this difficulty in more detail.

The dual frequency method is not susceptible to this problem. Mixed frequencies, $(f_1 + f_2)$ and $(f_1 - f_2)$, are produced only with the large amplitude whole body oscillations that occur around resonance. Therefore, since mixed frequencies are not simply a scattering phenomenon, it becomes unimportant that multiple scattering may be occurring. The mixed frequencies are dependent on the bubble's resonance frequency, f_R, and become $(f_1 + f_R)$ and $(f_1 - f_R)$. So a signal received at these frequencies indicates a bubble with resonance frequency, f_R, is in the sound field. Even though

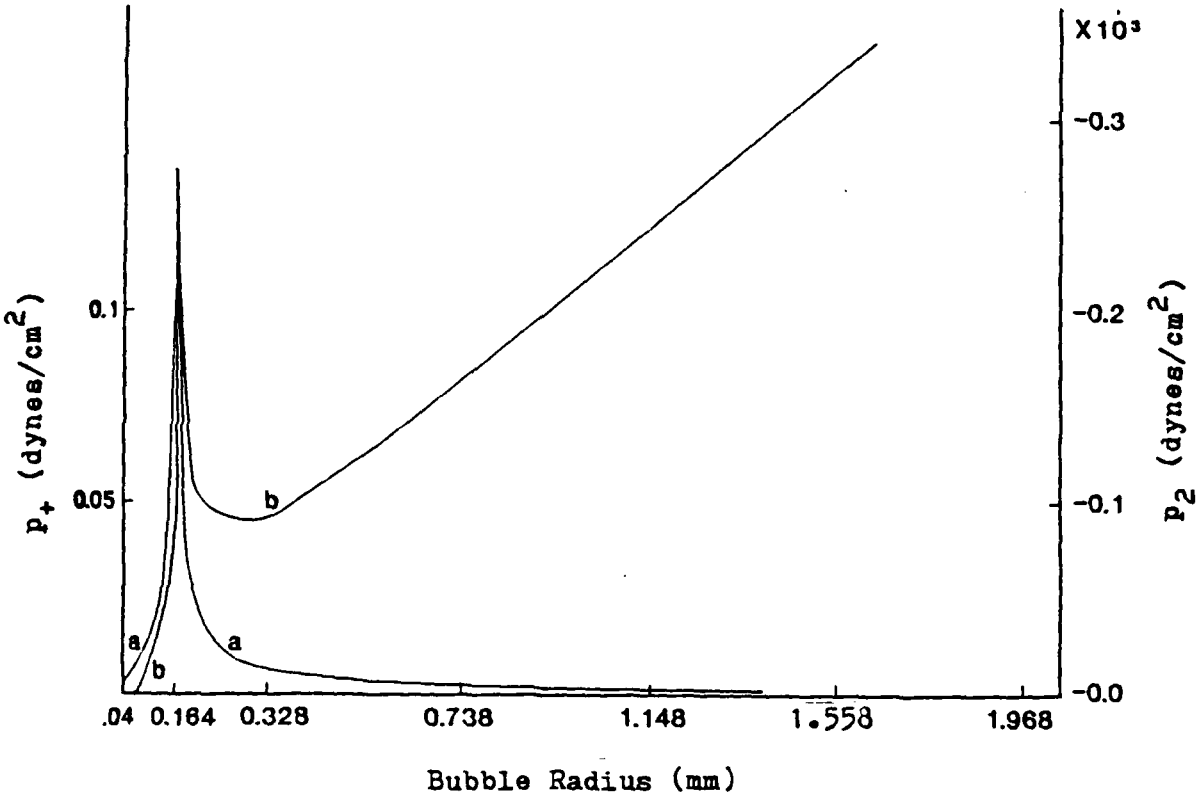

Figure 2 Comparison of the Dependence of Sum Frequency Pressure, p_+, and Exciter Frequency Echo Pressure, p_2, on Bubble Radius, Curve a: p_+ and Curve b: p_2

the scattered signal amplitude peaks, dips and then rises in a ramp fashion above the peak as bubble radius increases, as shown in curve b of Figure 2, the sum frequency signal is strong for only one bubble size, as shown in curve a.

2. Dual Frequency Interaction for Solids and Non-Resonant Bubbles

Beyer [Ref. 4] has gathered a lot of information concerning the nonlinear interaction of dual frequency sound fields. In this compilation of results from his own work and others, he presents information on the generation of sum and difference frequencies by the interaction of the fluid medium alone, a solid in the fluid and a bubble in the medium. These treatments allow us to estimate a maximum expected signal for cases without resonant bubbles.

a. Sound Interaction with Sound

In an experiment by Jones and Beyer it was shown that no sum or difference frequency is generated when two sound beams cross at right angles. In fact, sum and difference frequency signals are generated only when the beams are collinear. This case is termed the "parametric end fired array." It results in a highly directional sound beam. The pressure of this sound beam is proportional to the pressures of the primary frequency signals and the frequency separation between these signals. To produce the signal, the sound beams must be collinear for some distance. As a rule this process is less than one percent efficient.

b. Sound Interaction with Solids

The first effect to consider in the presence of a solid is scattering. The direction of scatter depends on the size, shape and orientation of the solid. To consider the parametric end fired array, assume that significant portions of both carrier and exciter are scattering toward the receiver. Although the receiver is very close to the sample volume, some interaction may occur during the interval. The resultant signal would have, at most, less than one percent of the scattered power. This power estimate is generous considering the short interaction length.

The second effect of solids in a dual sound field is their motion due to the radiation forces of the two sound fields. The motion of the solid induces the sum and difference frequency in the medium it contacts. To have this effect, the sound fields must be significantly intense to move solids at both the carrier and exciter frequencies.

c. Sound Interaction with Non-Resonant Bubbles

Beyer gives theory and experimental results for an air bubble interacting with dual frequency sound. The frequencies used were so high (5 and 7 MHz) that the bubbles were not resonant at these frequencies. The theory considers the interaction of sound scattered by the bubble. Scattering is the primary interaction for bubbles larger than resonance size. For the case presented, a 35 μm bubble is ensonified by 7 MHz at 2.45×10^5 Pa and 5 MHz at 3.36×10^5 Pa. These

frequencies are scattered omnidirectionally. The resulting pressures 48 cm away are 7 Pa and 6 Pa, respectively. The sum signal arrives with a pressure of 0.07 Pa.

This is interesting compared to the same analysis for a solid sphere. Here the sum frequency pressure is proportional to the square of the solid particle's radius and varies with direction. The maximum sum frequency signal exists directly down range from the sphere on a line with either source transducer. For a sphere over 90 times larger than the bubble mentioned above and identically ensonified, the maximum sum frequency pressure was 0.007 P_a at these two points. The minimum signal was between these points at a pressure of 0.00007 Pa. The placement of the receiver between the two sources ensures that we avoid the maximum values of the scattered signal pressure.

d. Overall Analysis of Solid Interference

Clearly there is a limit to the amount of solid material that can pass through the dual frequency sample volume without great effect. Much, however, can be said for this method's insensitivity to solids. First, the above experiments were performed at greater drive pressures than required for the dual frequency method. Lowering the drive pressures lowers these nonlinear effects. Second, note that the solid has much less sum signal than the non-resonant bubble. The non-resonant bubble has much less sum signal than the resonant bubble, as shown in Figure 2. It follows that

a solid particle will have a sum signal that is much less than that for a resonant bubble. This provides the means for discrimination between bubbles and solids.

The final argument to separate the resonant bubble's sum frequency signal from those of scattering phenomena is the frequency selectivity. The excitation signal is relatively low power over a broad band. Whereas the solid would scatter all frequencies uniformly, the bubble will be fundamentally excited by the presence of its resonance frequency. The whole body oscillations then mix the bubble's resonance frequency with the high power carrier. This sum and difference frequency signal will be easily distinguished from the other noise.

C. ADVANTAGES AND DISADVANTAGES OF THE DUAL FREQUENCY METHOD

The dual frequency method for bubble detection and resonance frequency determination has its good and bad points. The following is a quick summary of some of the key issues.

* Advantages
  - conclusive resonance frequency determination
  - discrimination between solids and bubbles
* Disadvantages
  - complexity of implementation
  - lower signal to noise levels than direct resonance frequency methods

* Other Effects

  - rectified diffusion
  - radiation pressure

1. Advantages

The foremost advantage of dual frequency bubble size determination is the single peaked response shown in Figure 2. Since this is not a simple scattered sound measurement technique, scatterers do not dominate the results. Large bubbles respond at their resonant frequency. They do not generate the same signals as small bubbles. This advantage is the same reason why solids do not give false detections.

Since this is an acoustic method using actual resonance phenomena, true resonance frequencies of skin covered bubbles can be determined by experiment. This could be important for certain types of plankton or other resonant scatterers. The contribution of the skin need not be calculated or assumed.

2. Disadvantages

One disadvantage is the complexity of the experimental set up and support equipment. Function generators must be capable of producing colored noise and narrow band high frequency. Frequency spectral analyzers must be capable of quickly and repeatedly analyzing the received signal over a wide range of frequencies. The transducers must be placed correctly to overlap the sound fields and receive a signal.

The second major disadvantage is the relatively low signal to noise level. The amplitudes of the sum and difference frequency signals are very small compared to the amplitudes of the signals received at the carrier and excitation frequencies. The sum and difference frequency generation mechanisms are nonlinear interactions and weaker than the linear interactions.

3. Other Effects

Another problem might be that the sound field could change the nature of the bubble being sized. Rectified diffusion, a process by which an oscillating bubble actually grows, will change the resonance frequency. Then the detected resonance frequency would not be the original undisturbed frequency. Crum [Ref. 5] gives a detailed discussion of the subject of rectified diffusion. The pressure amplitude necessary to initiate rectified diffusion is [Ref. 5:eq. 19:p. 217]

$$p_{TH}^2 = \frac{(\rho a^2 W_R^2)^2[(1-(W^2/W_R^2))^2+\delta^2 W^2/W_R^2][1+(2\sigma/ap_\infty)-c_i/c_o]}{(3+4K)(c_i/c_o)-\{[3(n-1)(3n-4)/4]+(4-3n)K\}[1+(2\sigma/ap_\infty)]}, \quad (3)$$

where,

w = frequency of excitation

σ = surface tension of the liquid

p_∞ = ambient pressure

c_i = concentration of dissolved gas in the fluid far from the bubble

c_o = equilibrium concentration of gas in the fluid

K = thermal conductivity of the gas in the bubble

n = polytropic exponent

p_{TH} = threshold acoustic pressure at excitation frequency.

Table 5 shows the results of some lengthy computations using Equation 3. Comparing the actual pressures used to these threshold values verified that rectified diffusion was not a problem with this experiment. The other saving point is that rectified diffusion takes hundreds of seconds to cause an appreciable change in bubble size as shown in [Ref. 5:Fig. 7:p. 222]. This is much longer than bubbles are expected to remain in the sound field.

Radiation force and streaming are two nonlinear effects discussed in Reference 4. These mechanisms have effects on the bubbles transiting the dual frequency sound field. The radiation force causes the bubbles to move away from the regions of high acoustic pressure. Streaming causes the bubbles to move away from the source transducers when in the sample volume. These motions make it difficult to maintain a small bubble in a small sample volume long enough to detect it. The effect of both of these mechanisms can be reduced by lowering the carrier and excitation pressure levels. Having a large sample volume with respect to the

TABLE 5. THRESHOLD PRESSURES FOR RECTIFIED DIFFUSION OF VARIOUS AIR BUBBLES IN AIR SATURATED WATER ($C_1/C_o = 1$)

Bubble Radius (μm)	Resonance Frequency (kHz)	Threshold Pressure (Pa)	Frequency (kHz)
100	31.4	1438	31.4*
50	62.1	2535	62.1*
10	303.8	8676	303.8*
5	618.0	1515000	2650.0**

* $W/W_R = 1$

** = carrier frequency

distance a bubble moves under the influence of these forces would also mitigate their effect.

D. BUBBLE RISE TIME SIZING

In order to verify that a bubble's acoustically indicated size is correct, some other method of determining the bubble size is necessary. A relatively easy, straightforward and accurate method is to measure the rise time of the bubbles as they rise through a known distance in still water under the influence of buoyancy. Reference 6 has documented this technique.

Essentially, a bubble rises at constant speed due to the balance between its buoyancy and its drag. These forces have different dependencies on radius. Hence, the rise speed of bubbles varies with radius; the larger the bubble, the faster it rises. The terminal rise speed of a bubble is given by [Ref. 6]

$$U = \left[\frac{8\ a\ g}{3\ C_D} \right]^{\frac{1}{2}}, \qquad (4)$$

where,

U = rise speed

g = acceleration due to gravity

C_D = drag coefficient

The values determined for time to rise one inch for various bubble sizes are shown in Table 6. The Schiller and Nauman drag law was used for these computations as given by Equation 5 [Ref. 6:eq. 4:p. 6].

$$C_D = \frac{24}{R_e}(1+0.15R_e^{0.687}) \qquad (5)$$

where,

R_e = Reynold's number = $2aU/V_f$

V_f = kinematic shear viscosity of fluid

In practice, there are a few difficulties with this method. The experimenter must be able to monitor the moving bubble. Thirty micron radius bubbles are about the smallest easily timed, with good lighting and clear water. There is some parallax since the scale cannot be extremely close to the rising bubble. With large bubbles, which move fast, observer response time is a factor. The experimenter cannot be 100 percent certain that the bubble timed is not accompanied by other bubbles that effect the acoustic output.

Overall, the rise time method is helpful. It allows at least a rough comparison of the acoustically determined resonance frequency with an expected value for

TABLE 6* TIME TO RISE ONE INCH FOR VARIOUS BUBBLE SIZES

Bubble Radius, a (μm)	Time to Rise One Inch (sec)
100	1.44
70	2.55
50	4.61
40	6.95
30	12.0
20	26.5
10	105
9	129
8	163
7	213
5	416

* The data in this table is included in the Easy Reference Table in the Appendix.

those bubbles that can be timed. Even when it cannot be used for every bubble, it gives the experimenter confidence in the dual frequency method.

III. PROBLEM APPROACH

The goal of this thesis is to develop and test a system which uses the dual frequency method to detect and size bubbles. In order to accomplish this goal, the following capabilities had to be incorporated into the experimental system.

* A method of generating bubbles and placing them in the sample volume.
* A method of placing solid particles in the sample volume.
* A method of producing a sound field of sufficient pressure amplitude.
* A method of receiving the pressure signals from the bubble and determining the frequency spectrum of that signal.

These methods are discussed in this chapter.

A. BUBBLE GENERATION

A method for generating bubbles of very small size is necessary for this study. Two basic generation methods were tried. In the first, bubbles were generated by pressurizing a pipette, made from a glass rod with a very narrow axial hole. The pipettes were very delicate, produced an audible sound during bubble generation and produced bubbles much larger than desired for this study. For these reasons, this method was abandoned and an electrolytic method was developed. Figure 3 shows the basic bubble production setup.

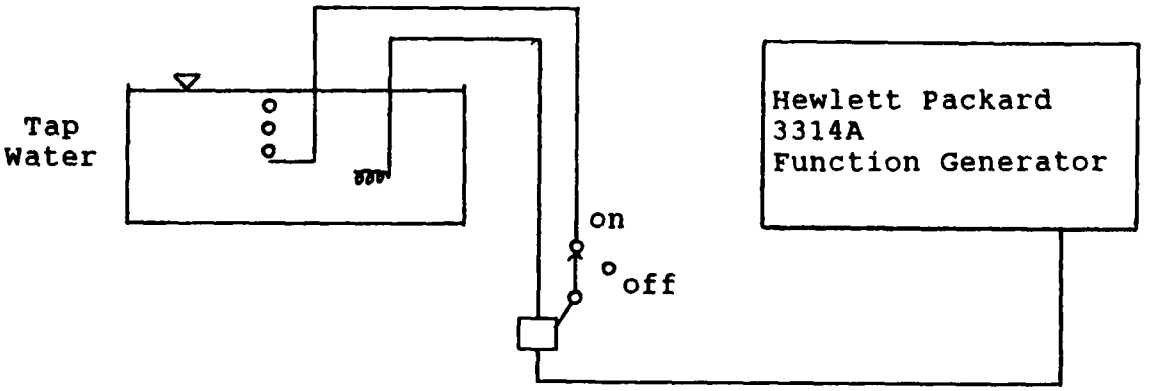

Figure 3 Electrolytic Bubble Generation Setup

Using the arbitrary (ARB) wave function mode on the Hewlett Packard (HP) 3314A, a negative electrical pulse was generated. The pulse was applied to a small wire, all but the very tip of which was insulated. A return wire with a bare coil tip completed the circuit back to the function generator. Ordinary (and by no means pure) tap water served as the electrolyte between the two leads. Very small bubbles would form and rise from the small wire during the negative pulses.

The nature of the bubbles was easily varied, but not controllable. Because the small wire tip corroded and collected deposits rapidly with use, the bubble size and quantity would vary with time, even with all of the parameters held constant. The use of a non-corroding wire, platinum for instance, might have solved this difficulty.

The number of possible variations offered by this setup proved useful. By adjusting the time scale on the ARB cycle the bubbles could be made to appear in quickly recurring

bursts having small numbers of small bubbles or in groups having a large number of larger bubbles with a larger interval between groups. As a rule to obtain smaller bubbles: (1) use a thinner wire, (2) use a shorter duration negative pulse, (3) use a lower voltage negative pulse. Conversely, larger bubbles were more likely with thicker wire, higher voltages and longer duration pulses.

It was impossible to generate only one size bubble over any length of time with this method. With several small bubbles present, two would often join to form a larger bubble. The larger bubble would then rise faster, overtake and join another bubble. To prevent this, an on-off switch was placed in the circuit. The current was interrupted after a bubble was formed to limit interference with other bubbles.

1. Variations of Bubble Control

a. Grid

Since the position of the rising bubbles is important to this experiment, some way is desired to move the generation point a known amount. One solution is a grid of 32 wires terminating on a small blank circuit board. Arranged in 4 columns and 8 rows with the tip of each wire about one millimeter from its neighbor, the source of bubbles could be moved by switching one wire off and another on. Also a massive cloud of bubbles could be achieved by turning on all or some of the wires at the same time.

b. Bubble Size Discrimination Plate

In order to narrow down the size range of bubbles which passed through the sound field, a small horizontal water jet was produced near the bubble generator. The jet was established by connecting a water reservoir to a small hollow glass tube. The speed of the jet could be controlled through the height of the reservoir. As bubbles were generated they were swept downstream by the jet. The length of travel was inversely proportional to the size of the bubble. Eventually the bubbles would rise out of the jet and continue up to the surface. A plastic plate with one small hole was placed above the jet. This arrangement allowed only those bubbles leaving the jet at the position of the hole to rise through the sound field, as shown in Figure 4. Although helpful in narrowing down the range of bubble sizes, some variation was still apparent.

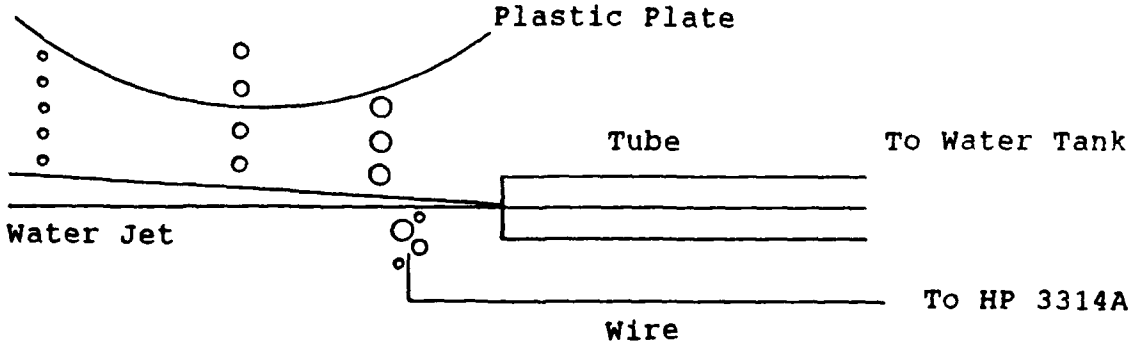

Figure 4 Bubble Size Discriminator Plate

c. Blow Pipe

There are a number of difficulties associated with getting very small bubbles into the sound field. Worst of all, they are just about impossible to see. They drift away from the acoustic sample volume very easily, and they rise at very slow speeds, several minutes per inch. In order to get them into the sample space, they had to be convected. To this end, the bubbling wire was inserted into a narrow glass tube. The tube was pressurized by a water reservoir with about one foot of static head. The water was allowed to flow continuously while the bubbles came in short pulses. The tube could be (relatively easily) positioned so that the convected bubbles would pass through the sample volume.

B. SOLID INJECTION

In order to show that the frequency mixing due to solid particulates in the system is dramatically different from that due to bubbles, and that therefore the system would show the ability to discriminate between a bubble and a solid, such solid particles had to be introduced into the sample volume.

Three basic types of solid particles were injected. The first, dry sand, was dropped directly over the dual sound field via a dry funnel and allowed to fall to the tank bottom. It was never certain whether the particles fell directly through the most intense portion of the sound field or not, due to their long fall and fluttering motion.

Wet sand was injected in a water slurry via a long wet funnel terminating just above the dual sound field. Wetting the sand prior to injection reduced the number of visible bubbles entrained with the sand.

Thin wall hollow glass beads were also injected into the sound field. Due to their extreme buoyancy they had to be convected. A glass tube was aimed at the dual sound field horizontally and pressurized with a bead slurry. The beads would pass into the sound field horizontally and rise to the surface. The glass beads ranged in size from about 5 to 50 μm radius, as determined by microphotography. The sand particles ranged from 1 μm to 1 mm in largest dimension.

C. TRANSDUCER CHARACTERISTICS AND CONFIGURATION

Due to the range of frequencies used in this experiment several types of transducers were needed. The lower frequency driving transducer, called the exciter, needed significantly different parameters than the higher frequency driving transducer, called the carrier. Since the sum and difference frequencies were close to the carrier frequency, the receiving transducer, or receiver, was very similar to the carrier transducer. Other transducers were used for special purposes, such as calibration, but were not part of the dual frequency system. This section will present each transducer's characteristics and the methods used to determine those characteristics.

1. Types of Transducers

Two 6 cm diameter focused piezoelectric transducers were used for the carrier and receiver. They were chosen for the acoustic gain advantage of focusing. The acoustic pressure at the focus is many times that at the face of the transducer. The serial numbers of these transducers are C5575 and C5574. They were manufactured by Harisonic. Nominal specifications include a 2.25 MHz resonance frequency and a 3 inch focal length.

A Panametrics V301 3 cm diameter circular piezoelectric disk transducer was used as the exciter. This choice was made since it had good frequency response over the range of 30 to 400 kHz. This transducer had a source strength that mainly increased with frequency over this range. That was ideal for this purpose. The serial number of this transducer was 93598. To assist in reciprocity calibration a similar transducer, serial number 93596, was used.

To determine the transducer beam patterns and assist in correctly positioning the transducers in the system, a very small hydrophone, made by Specialty Engineering, was used. The hydrophone looks like the tip of a very sharp pencil, with all dimensions of the ceramic receiver less than a millimeter. A preamplifier supplies enough signal boost to give significant oscilloscope readings. This hydrophone was used to probe the sound fields for relative measurements. No attempt was made to calibrate the probe.

Finally, an EDO corporation model 6600 spherical piezoelectric hydrophone was used for the reciprocity calibration of the exciter.

2. Beam Patterns

The beam patterns of the exciter, carrier and receiver are important since their intersection determines the size of the sample volume. Also, an accurate knowledge of the beam pattern is crucial to the calibration of the focused transducers. The methods used to measure the beam patterns of the transducers are described in this section.

a. Beam Pattern Method

In order to obtain an accurate beam pattern, the transducer and probe hydrophone were mounted to a common frame via a network of micrometer positioners. Thus, the probe could be moved known distances, relative to the transducer, in small steps. The setup allowed relative motion in the three orthogonal directions of vertical, range and cross range.

The first step in measuring the beam patterns of the focused transducers was to locate the position of the focus. Then readings of distance and probe output voltage were taken relative to the focus. At any given frequency, the probe output voltage was assumed to be proportional to the acoustic pressure at the probe. Normalized pressure values were obtained by dividing each value in a data set by the maximum value in that data set.

The exciter beam pattern was much broader than those of the focused transducers. Cross range data for the exciter was taken at a few ranges of interest. Since the exciter's beam pattern is, theoretically, narrower at higher frequencies, the data was taken at 400 kHz. This verified proper coverage at the highest exciter frequency of interest. The patterns at lower frequencies were then guaranteed to be sufficiently broad.

b. Beam Pattern Results

At 400 kHz the exciter had a very smooth beam pattern. At a distance of 4.0 cm the 3 dB beam width was about 1.0 cm. Figure 5 shows the normalized pressure versus cross range at a range of 4.0 cm. The variation of pressure with range was minimal for ranges 4 cm to 6 cm. At a range of 10 cm the maximum pressure was approximately 3 dB less than that at 4.0 cm range. Figure 6 shows the area within which the pressure was greater than the 3 dB less than the maximum value (0.71 p_{max}). As will be shown below, this beam pattern is sufficient to ensonify the intersection volume of the carrier and receiver, which limited the size of the sample volume.

The beam patterns of the focused transducers were much more complicated. The acoustic pressure changed rapidly with distance, especially at the focus. Figure 7 shows the variation of normalized pressure with range along the axis for

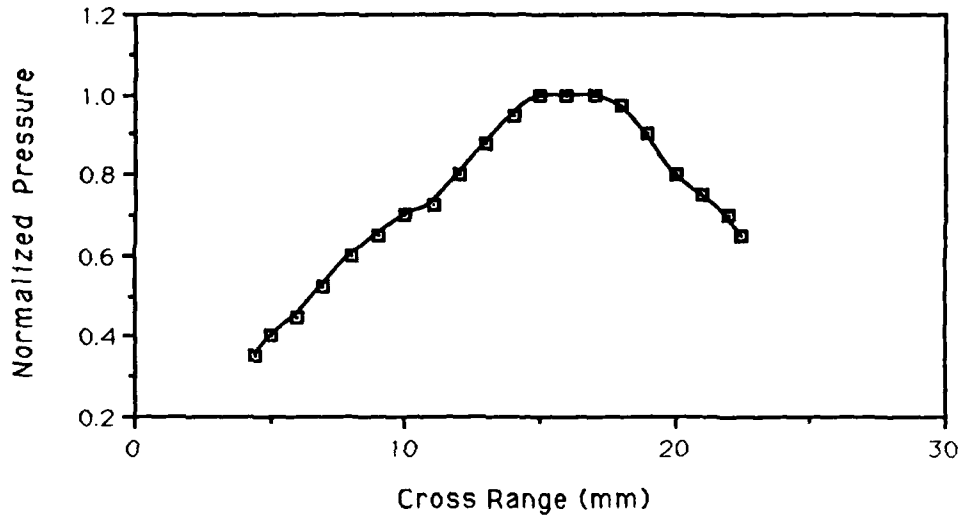

Figure 5 Exciter Cross Range Pressure Variation at a Range of 4.0 cm

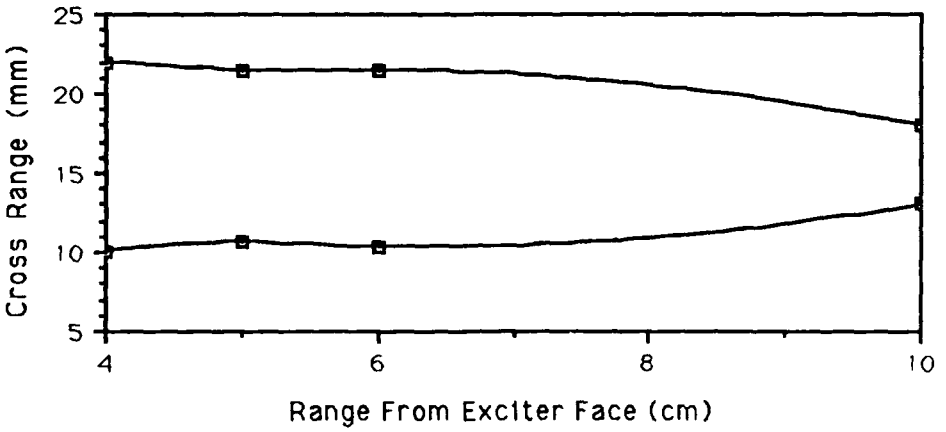

Figure 6 View of Exciter Main Beam. Area inside curves is High Pressure Region.

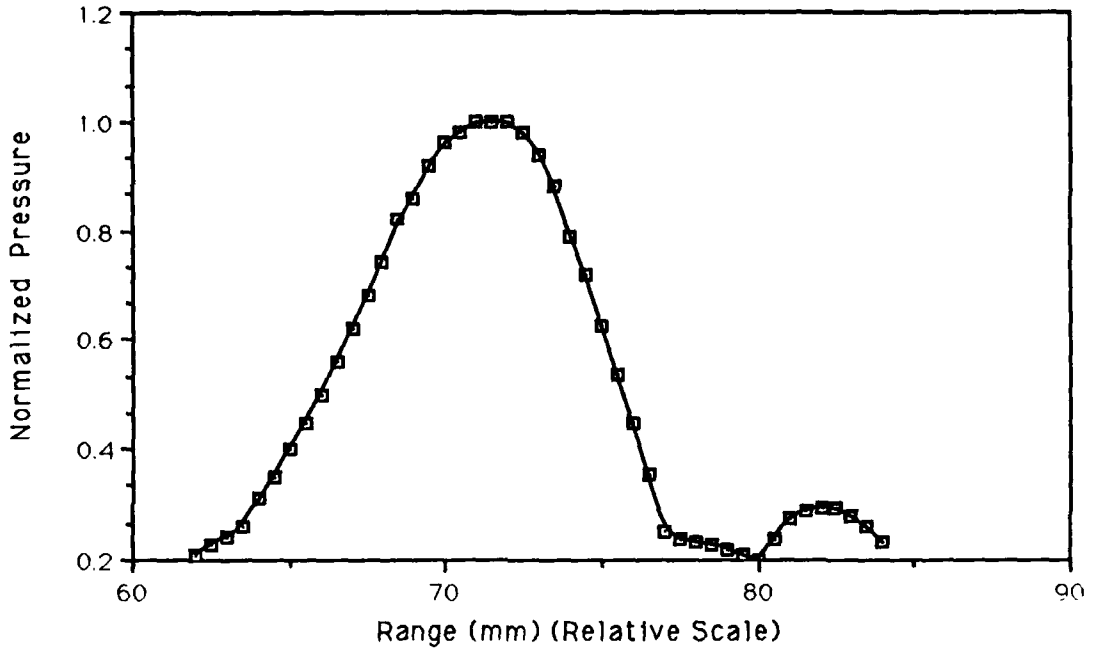

Figure 7 Focused Transducer's Pattern of Pressure versus Range at the Focus

transducer C5574. Both focused transducers were similar in this regard. At the focus, the pressure stays at or near the maximum for about 5 mm of range, and at least half of the peak value for 10 mm. Figures 8 and 9 show the vertical variations of normalized acoustic pressure at the focus of C5574 and C5575, respectively. The pressure stays at or near its maximum value for only 1 mm vertically. Comparing these graphs for the two transducers reveals that C5575 focuses a little tighter than C5574. The cross range beam patterns are very similar to the vertical patterns and are not shown. Although the beam patterns are axially symmetric in general, there are a number of small variations in the pressure field.

Figures 10 and 11 show the horizontal plane (cross range versus range) containing the focal axis for C5574 and C5575, respectively. Isobaric lines surround areas within which the pressure is at least as great as the isobaric pressure. This is just another way to show that pressure varies ten times faster with cross range than with range. To compare the graphs, note that although the isobaric lines are labeled differently in units of dB relative the maximum value for that plot, the inner oval for C5574 represents the same pressure as the inner oval for C5575. These plots were instrumental in understanding the focused transducers' sound fields. They provided key information for the calibration processes as shown in the next section. Further detailed

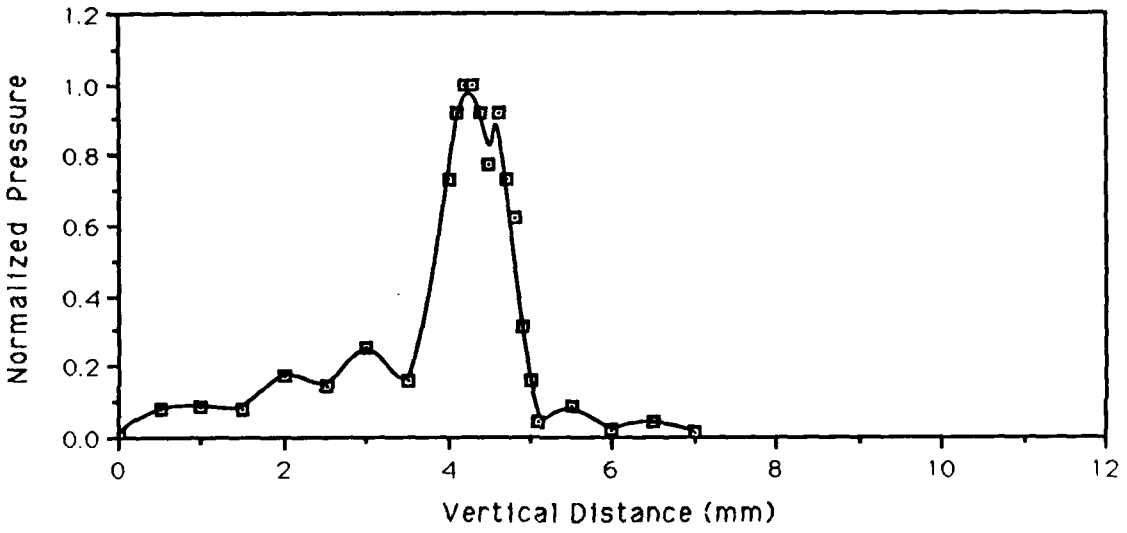

Figure 8 C5574 Vertical Variation of Pressure at the Focus

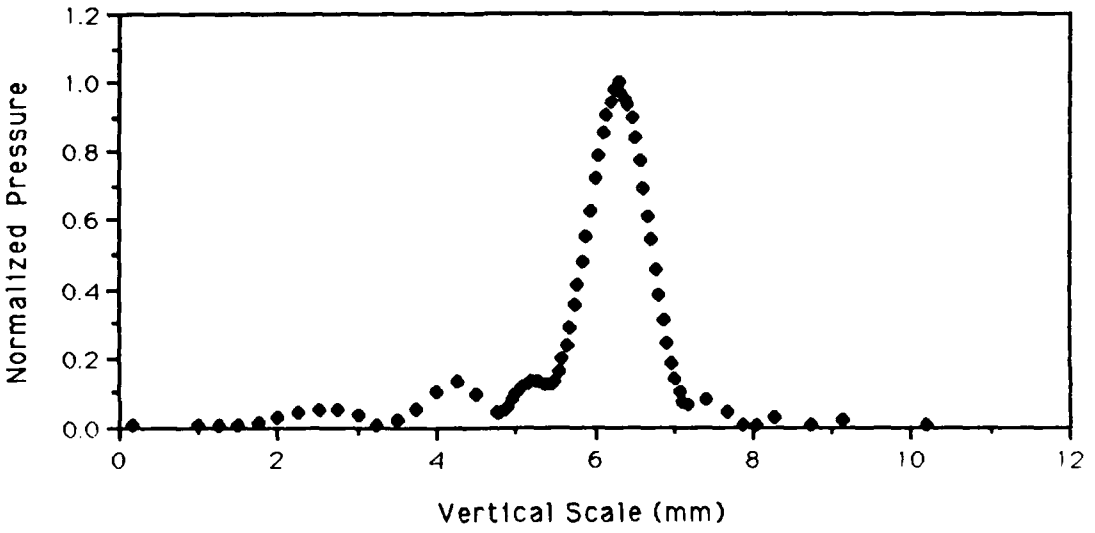

Figure 9 C5575 Vertical Variation of Pressure at the Focus

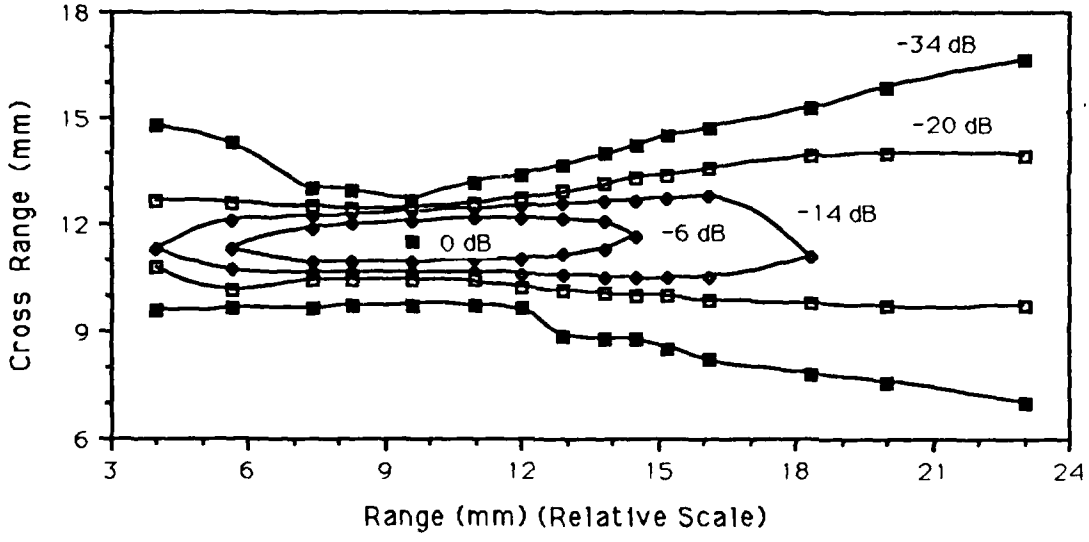

Figure 10 C5574 Horizontal Focal Plane Pressure Distribution

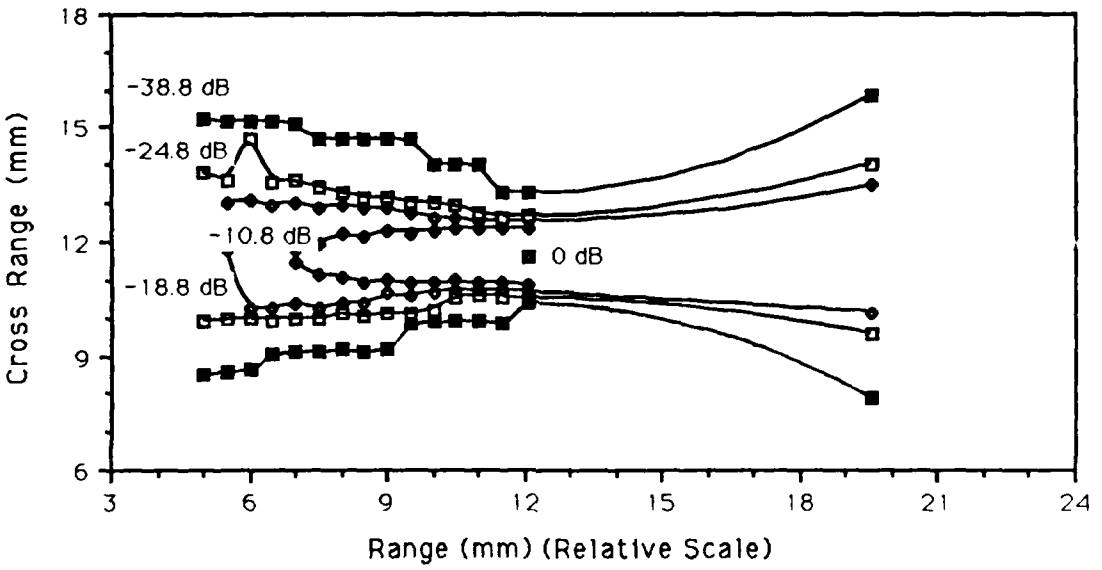

Figure 11 C5575 Horizontal Focal Plane Pressure Distribution

analysis of the resulting sample volumes is given after the calibration section.

3. Transducer Calibration

The beam patterns in the previous section were all plotted relative to some maximum value for that transducer. To apply the dual frequency theory and calculate the expected sum and difference frequency signal pressures, the carrier and exciter pressures must be determined. Also the receiver sensitivity must be known. To this end, several calibration methods were used. This section presents a brief outline of each method and the results obtained.

a. Methods of Calibration

(1) Reciprocity. References 7 and 8 present a significant amount of information on reciprocity calibration of transducers. If done correctly, this type of calibration is a prime standard of transducer performance. The key to the reciprocity method is two fold, as Reference 9 points out. First, for a linear, passive and reciprocal transducer there is a simple relationship between the transducer's receiving sensitivity, M, and its transmitting response or source strength, S;

$$\frac{M}{S} = J, \tag{6}$$

where,

M has units of voltage/pressure

S has units of pressure/current

J has units of (voltage)·(current)/(pressure)^2.

J is called the reciprocity parameter and depends on the nature of the calibration method. Several methods of reciprocity calibration are presented in Reference 8 with their associated reciprocity parameter. The second key to the reciprocity method is that the beam pattern of a transducer is the same whether it is acting as a source or receiver. This property was assumed in order to determine the beam pattern of the receiver in the last section.

The full reciprocity method requires one transmitter, T, one hydrophone, H, and one reversible transducer, R. Three basic steps exist in the experiment. First, place the transmitter, T, a known distance, d, from H. Record the open circuit voltage response from H, V_{HT}, for a known current, i_t into T Second, replace H with R. Record the open circuit voltage out of R, V_{RT}, for the same current into T. Third, replace T with R and return H to its original position. Record the open circuit voltage out of H, V_{HR}, for a known current, i_R, into R The hydrophone sensitivity, M_H, can be calculated according to

$$M_H = \left[\frac{V_{HT}\, V_{HR}}{V_{RT}\, i_R} J \right]^{\frac{1}{2}}, \qquad (7)$$

where,

J = $2\lambda d/\rho_o c$, for spherical spreading

λ = acoustic wavelength

$\rho_o c$ = characteristic impedance of the medium.

A transducer's source strength, S, is a measure of how much pressure, p, it produces at a distance of one meter for a given current, i. When p is measured at a distance, d,

$$S = \frac{p}{i} \frac{d}{1(m)}. \qquad (8)$$

Sensitivity, M, is a measure of the open circuit voltage, V, produced for a given pressure, p, at the transducer face,

$$M = \frac{V}{p}. \qquad (9)$$

For this reciprocity calibration it is assumed that the hydrophone is small enough to not disturb the sound pressure field. Thus, the pressure in the above two equations can be equated, giving

$$S = \frac{V}{Mi} \frac{d}{1(m)}. \qquad (10)$$

This equation is used to calculate the exciter's source strength after the EDO hydrophone's sensitivity is determined.

(2) Two Transducer Reciprocity. A short cut can be made if two identical reciprocal transducers are to be calibrated. Here, only one transducer arrangement is required. The transducers are placed a known distance, d, apart. Then the open circuit voltage of one is measured while a known current is put through the other. The sensitivity and source strength of both transducers are given by Equations 11 and 12.

$$M = \left[\frac{V}{i} J \right]^{\frac{1}{2}} \quad \text{and} \quad S = \frac{M}{J} \qquad (11 \text{ and } 12)$$

The disadvantage of this method is that the transducers must be exactly identical in sensitivity and source strength. This must be shown by another method before the two transducer reciprocity becomes valid.

(3) Self Reciprocity Method. A third variation on the reciprocity method involves only one transducer. This method is very similar to two transducer reciprocity, except that there is no longer the need for identical transducers. The transducer is aimed at a perfect reflector, such as an

air-water interface. A pulse of known current is put through the transducer. The acoustic pulse is reflected from the interface and returns to the transducer. The open circuit voltage amplitude of the received pulse is recorded. Care must be taken to ensure the transducer is aimed correctly to receive the reflected pulse. The source strength and sensitivity equations are identical to those for the two transducer methods. Since the transducer remains connected to the pulse generator while measuring the return voltage, a diode or other high impedance arrangement must be used to isolate the influence of the pulse generator's low impedance on the open circuit voltage measurement.

(4) Radiation Force Target Deflection. In this method, a perfectly reflecting target is hung in the transducer's sound field. The target is deflected due to the radiation force. The amount of deflection is determined by the balance of the radiation force and the weight of the target. As shown in Reference 10, the total acoustic power, Π, acting on the target is determined by the deflection distance, e, multiplied by a target specific factor, as shown in Equation 13.

$$\Pi = \frac{mgc}{L} e \qquad (13)$$

where,

m = mass of the target

g = gravitational acceleration

c = speed of sound

L = length of target suspension

e = deflection distance.

At the focus, the total acoustic power is given by Equation 14.

$$\Pi = \int I_F \, dA_F \tag{14}$$

where,

I_f = intensity of the sound over the infinitesimal area, dA_f

dA_f = infinitesimal area in a plane intersecting the focus and perpendicular to the transducer's axis

The intensity is related to pressure, for plane or spherical waves, by Equation 15.

$$I = \frac{p^2}{\rho_o c} \tag{15}$$

so,

$$\Pi = \int \frac{p_F^2}{\rho_o c} \, dA_F \tag{16}$$

Now, define s(x) as the pressure's radial shape function which equals the normalized pressure at a vertical or cross range distance, x, from the focus. In other words, this shape function looks exactly like Figure 8 for C5574 or Figure 9 for C5575. The pressure at a radial distance, x, in this focal plane, $p_f(x)$, can be written in terms of the maximum pressure and the radial shape function as in Equation 17.

$$p_F(x) = p_{FMAX}s(x) \tag{17}$$

substitution gives,

$$\Pi = \frac{p_{FMAX}^2}{\rho_o c} 2\pi \int_0^\infty s^2(x)\ x dx \tag{18}$$

$$\Pi = \frac{p_{FMAX}^2}{\rho_o c} A_{eff} \tag{19}$$

A_{eff} is the effective beam area at the focus. It is obtained by numerically integrating the shape function squared over the focal plane.

Substituting the target deflection parameters for Π and solving for maximum focal pressure yields Equation 20.

$$p_{FMAX} = \left[\frac{\rho_o c^2}{A_{eff}} \frac{mge}{L} \right]^{\frac{1}{2}} \tag{20}$$

In order to compare this result to that of the self reciprocity method, the pressure at the transducer face (determined from the source strength) must be converted to the pressure at the focus. The conversion is made assuming the acoustic energy at the face equals that at the focus. This assumption yields

$$p_{FMAX} = \left[\frac{p_T^2 A_T}{A_{eff}} \right]^{\frac{1}{2}}, \qquad (21)$$

where,

A_T = area of the transducer face

p_T = pressure at the transducer face.

b. Calibration Results

Some of the methods described in the previous section were more suitable than others depending on the particular transducer to be calibrated. For instance, the full reciprocity method was ill suited for the focused transducers because of the rapidly varying pressure pattern in the focused sound field and the high frequency. Under these circumstance, the assumption that the hydrophone does not disturb the pressure field is not valid. The other tree methods were viable alternatives. For the exciter, the Self Reciprocity and Radiation Force Target Deflection methods were not used because of the low pressure amplitudes.

(1) Exciter Calibration. A full reciprocity calibration was performed on the exciter, using a second transducer of the same design (twin) and an EDO hydrophone. This type of calibration results in a value for the hydrophone's receiving sensitivity. The exciter's source strength can then be calculated by Equation 22.

$$S_E = \frac{V_{EDO}}{M_{EDO}\, i_E} \frac{d}{1(m)} \qquad (22)$$

where,

S_E = exciter's source strength

V_{EDO} = open circuit voltage of EDO hydrophone

M_{EDO} = EDO hydrophone's receiving sensitivity

i_E = current input to exciter

d = distance between source and hydrophone

The calibration was performed twice at each frequency to get two values for the EDO's sensitivity. To make the two values somewhat independent the roles of projector and reciprocal transducer were exchanged between the exciter and its twin. The values for the EDO's sensitivity were averaged and compared with expected values provided from the manufacturer. The average EDO sensitivity was used in all computations.

The source strengths of the exciter and its twin were calculated using Equation 22. At some frequencies

the source strengths of the exciter and its twin were close to identical. The two transducer reciprocity calibration was performed twice in that case. Again, the roles of source and receiver were switched to provide some small degree of independence between the two runs. For this method the source strength is given by Equation 23.

$$S = \left[\frac{V}{i\ J} \right]^{\frac{1}{2}} \tag{23}$$

where,

V = open circuit voltage of the receiver

i = input current to the source

J = reciprocity parameter, $2\lambda d/\rho_o c$

λ = acoustic wavelength

For these calibrations, the received open circuit voltage was measured directly on an oscilloscope having a 1 megaohm input impedance. The input current was determined by measuring the voltage across a 10.1 ohm resistor, placed in series with the driving transducer, on another channel of the same oscilloscope. The drive signal was obtained from a Hewlett Packard (HP) 3314A Function Generator.

The full reciprocity method seemed to be the most reliable of these calibrations. The full reciprocity calibration results for the exciter were used in all further

equations requiring exciter source strength. Since the exciter was used for the full continuum of frequencies from 30 to 400 kHz, it was calibrated at 50 kHz intervals from 50 to 400 kHz. Table 7 contains the results of these calibrations.

The true matter of interest is the pressure in the sample volume, which is obtained from Equation 8 rearranged as $p = s\, i \cdot 1(m)/r$. The drive current is determined by measuring the voltage across the 10.1 ohm resistor as discussed earlier. However, the drive signal is broadband noise. The oscilloscope cannot be used to determine voltage at a chosen frequency in this case. The voltage (rms) was measured with the HP 3585A Spectrum Analyzer. The peak current is therefore given by Equation 24.

$$i = \frac{\sqrt{2}\, V_{rms}}{R} \qquad (24)$$

Using this expression the pressure is found to be,

$$p = \frac{\sqrt{2}\, V_{rms}\, S \cdot 1(m)}{R \quad r} \,, \qquad (25)$$

TABLE 7 EXCITER CALIBRATION RESULTS.
SOURCE STRENGTH IN UNITS OF Pa/mA

	FULL RECIPROCITY		TWO TRANSDUCER METHOD	
FREQ. (kHz)	S(EXCITER)	S(TWIN)	S(EXCITER)	S(TWIN)
50	310	526	--	--
100	1440	1160	--	--
150	1860	2510	--	--
200	3340	3250	3380	3440
250	5160	5300	5400	5460
300	11100	5560	--	--
350	11300	10300	11200	11200
400	13600	13700	14200	14200

where,

V_{rms} = voltage determined by spectrum analyzer

R = resistance of series resistor

r = distance from the transducer face to the sample volume

Table 8 gives the values of peak pressure for the maximum noise signal used to drive the exciter during the experiments. It turns out that the exciter has some significant variation in output pressure over this frequency range. Interpolated values were used for frequencies of interest that were not part of the calibration.

(2) Focused Transducer Calibration. The first method attempted in the focused transducer calibration was the two transducer method. The position of both transmit and receive focused transducers were adjusted to maximize the return signal. This position turned out to be such that the transducers faced each other with the acoustic foci overlapping at half the distance between them, as shown in Figure 12. The two transducer method was performed twice. Switching the roles of source and receiver between C5575 and C5574. The obvious problem with this method was that it gave no indication of differences between the transducers. The result is a single number for source strength and another for sensitivity. It was suspected and later proven that the

TABLE 8* PEAK EXCITER PRESSURE AT 4 CM AT VARIOUS FREQUENCIES WHEN DRIVEN WITH MAXIMUM NOISE SIGNAL

Frequency (kHz)	Peak Pressure at 4 cm (Pa)
50	115
100	261
150	244
200	370
250	515
300	980
350	1000
400	1190

* The data in this table is included in the Easy Reference Table in the Appendix.

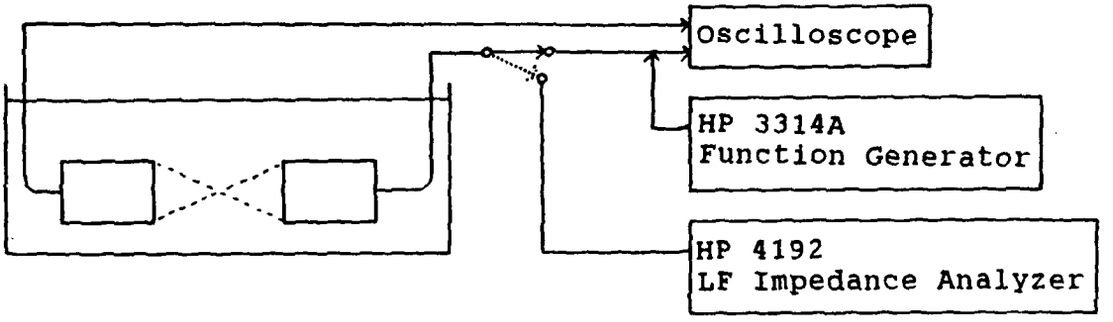

Figure 12 Two Transducer Reciprocity Calibration Using Focused Transducers

transducers were not identical. This calibration resulted in a ball park verification of other methods used.

Since the impedance of the focused transducers was not large compared to 10.1 ohms, and external resistor was not used in the determination of input current. Instead the magnitude of the free field impedance, $|z|$, of the source transducer was measured separately at the frequencies of interest using a HP 4192 LF Impedance Analyzer. With this value known, the input current could be deduced from the drive voltage. The receiving transducer's open circuit voltage was measured directly on the oscilloscope.

As stated previously, one key to any reciprocity calibration is the reciprocity factor, J. For small, omnidirectional sources in open water this factor is normally given by Equation 26.

$$J = \frac{2\lambda d}{\rho_o c} \tag{26}$$

where,

λ = acoustic wavelength

$\rho_o c$ = characteristic impedance of the medium

The distance factor, d, is included to account for losses due to spherical spreading. However, for the focused transducers, spherical spreading is not the case. The sound field converges to and diverges from a focal point.

On the average, this can be equated to a plane wave phenomena in the sense that the receiver intercepts essentially all of the acoustic energy produced by the transmitter. Reference 8 gives a brief presentation of plane wave reciprocity. Reference 11 provided a verification of the plane wave reciprocity factor given in Reference 8 and Equation 27.

$$J_p = \frac{2\lambda d}{\rho_o c} \tag{27}$$

where,

A = area of transducer face (curved area for focused transducers)

In order to avoid the need for identical transducers, the self reciprocity method was used. The transducer was positioned vertically underwater to achieve a maximum surface reflected signal. This placed the focal point at the air water interface as shown in Figure 13.

A pulse of about 200 cycles at the desired frequency in the range of 2.25 MHz to 3.10 MHz was generated by the HP3314A every 10 milliseconds. The drive pulse was powerful enough to pass through the diode network and drive the transducer under test. However, the diodes caused some minor signal distortion. To account for this, the drive signal was monitored on a spectrum analyzer at each drive frequency used. A ratio of signal voltage at the drive frequency as measured on the spectrum analyzer to the waveform

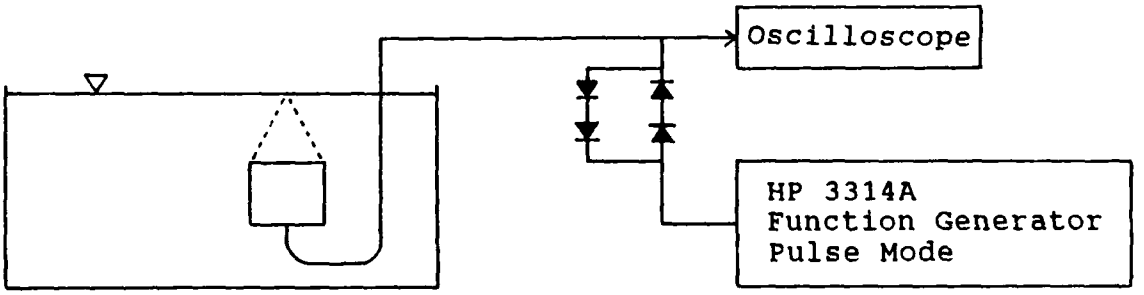

Figure 13 Self Reciprocity Method for Focused Transducers

peak to peak voltage as measured on the oscilloscope was calculated for each drive frequency. This ratio was used as a correction factor to the drive voltage measured on the oscilloscope.

The diodes essentially eliminated the HP 3314A's low impedance from the receiving circuitry. Because of losses to the diode circuit, the received voltage measured on the oscilloscope with the diode circuit installed was noticed to be about 99 percent of the open circuit voltage. A factor of 1.01 was used to correct the oscilloscope readings to open circuit voltage readings. Since the received signal was spectrally dominated by the desired frequency, a second frequency correction factor was not required.

Table 9 shows the results of this calibration. In general, C5575 was a more powerful source and a more sensitive receiver than C5574. Notice that the two transducer method result of 0.135 mV/Pa sensitivity at 2.65 MHz is not far from an average of the self reciprocity method results for the same frequency.

Note also the unexpected difference in the characteristic rolloff from the nominal resonance frequency of 2.25 MHz. C5575 shows an expected pattern of falling sensitivity with increasing frequency beyond this point. While C5574 stays virtually flat over the sum and difference frequency range. For this reason, C5574 was chosen to be the receiver. C5575 provided the carrier signal.

TABLE 9 SELF RECIPROCITY CALIBRATION RESULTS FOR THE FOCUSED TRANSDUCERS

	C5575		C5574	
FREQ. (MHz)	SENSITIVITY (mV/Pa)	**SOURCE STRENGTH (Pa/mA)	*SENSITIVITY (mV/Pa)	**SOURCE STRENGTH (Pa/mA)
2.25	0.244	58.3	0.0982	23.5
2.30	0.238	57.0	0.0969	23.2
2.35	0.236	56.6	0.0955	22.8
2.40	0.232	55.5	0.0951	22.7
2.45	0.232	55.5	0.0939	22.5
2.50	0.230	55.0	0.0936	22.4
2.55	0.230	55.1	0.0932	22.3
2.60	0.229	54.8	0.0934	22.3
2.65	0.227	54.4	0.0932	22.3
2.70	0.226	54.1	0.0937	22.4
2.75	0.224	53.6	0.0948	22.7
2.80	0.221	52.9	0.0947	22.6
2.85	0.217	52.0	0.0967	23.1
2.90	0.213	50.9	0.0966	23.1
2.95	0.207	49.4	0.0982	23.5
3.00	0.196	46.9	0.0974	23.3
3.05	0.186	44.5	0.0972	23.2
3.10	0.176	42.1	0.0966	23.1

* This data is included in the Easy Reference Table in the Appendix.

** at the transducer face

Of particular interest is the pressure of the carrier signal in the sample space. The maximum pressure at the focus, P_{FMAX}, is calculated from Equation 28 after determining the input current, i, and the effective acoustic area, A_{eff}.

$$p_{FMAX} = \left[\frac{(S_{2.65MHz} \times i)^2 A_T}{A_{eff}} \right]^{\frac{1}{2}} \qquad (28)$$

$$i = \frac{V_{pp}}{2|z|_{2.65MHz}} \qquad (29)$$

where,

V_{pp} = peak to peak voltage of drive wave form on the oscilloscope

$|z|_{2.65MHz}$ = magnitude of free field impedance of C5575 at 2.65 MHz

$S_{2.65MHz}$ = source strength of C5575 at 2.65 MHz

Since the carrier is monofrequency, the only parameter that varies is V_{pp}. Table 10 shows some calculations for P_{FMAX} based on some typical input voltages. The following values were used for this table. $S_{2.65MHz}$ = 54. Pa/mA, A_T = 3094.5 mm^2, A_{eff} = 0.6811 mm^2, $|z|_{2.65MHz}$ = 135.3 ohms.

TABLE 10* MAXIMUM PEAK FOCAL PRESSURE OF THE CARRIER AT 2.65 MHz FOR VARIOUS INPUT VOLTAGES AS DETERMINED BY THE SELF RECIPROCITY CALIBRATION

Voltage (Peak to Peak)	Maximum Peak Focal Pressure (Pa)
0.052	707
0.165	2242
0.41	5570
0.55	7472
1.10	14940
2.08	28260
2.55	34640
4.05	55020
5.2	70650
8.2	111400
10.35	140600
12.9	175300

* The data in this table is included in the Easy Reference Table in the Appendix.

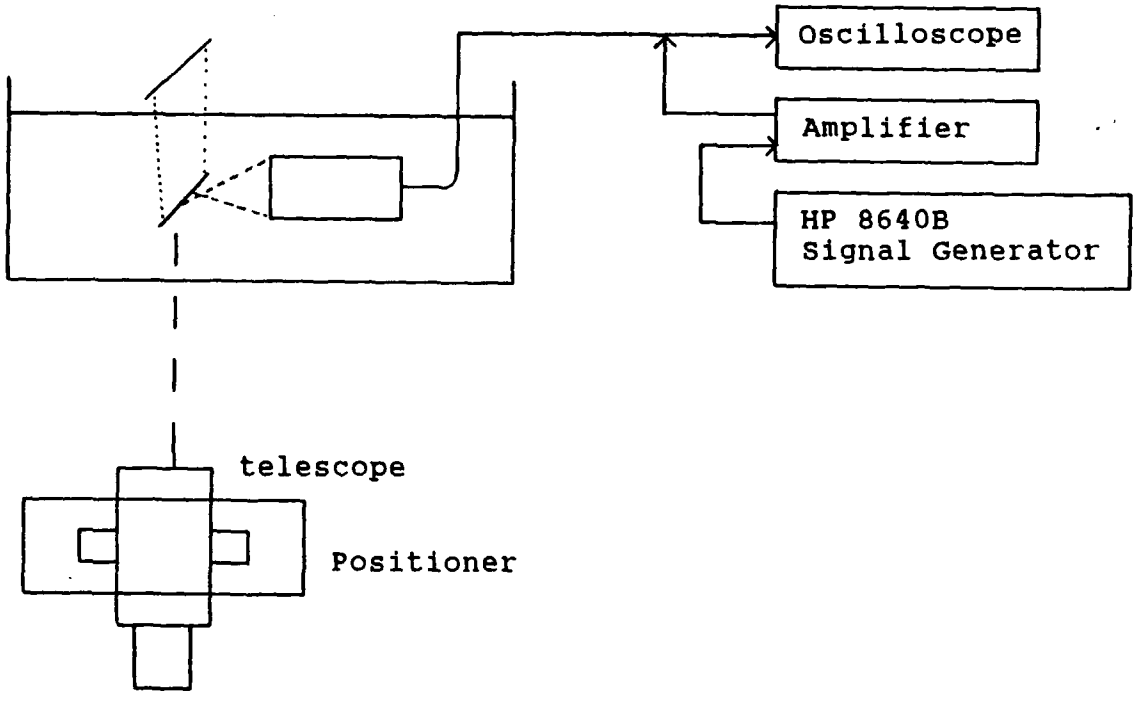

Figure 14 Radiation Force Target Deflection Calibration Setup

An additional calibration using the radiation force target deflection method was performed in order to verify the reciprocity calibration results. This test was easily performed using the setup shown in Figure 14. The target was positioned at the approximate location of the focus in order to intercept the entire signal. The deflection was measured with a telescope mounted to a micrometer positioner. The HP 8640B Signal Generator created the 2.65 MHz signal with very fine voltage control and spectral purity. Using Equation 20, Table 11 was generated using the deflection distances and input voltage data from this experiment. This determination of peak carrier pressure at the focus compares favorably with the self reciprocity method.

4. Test Setup and Sample Volume

Due to the highly focused beam patterns, precise alignment of the transducers was required. For this reason, the transducers were mounted to micrometer positioners which allowed adjustments of range, cross range and height. The alignment procedure consisted of first placing the probe hydrophone in the focal region of the carrier. The receiver was then carefully positioned so that its focus also coincided with the position of the probe. Similarly, the exciter was aimed at the probe to provide maximum excitation signal to the sample volume. The bubble generator was then positioned such that the bubbles impinged on the probe and thus would go

TABLE 11* MAXIMUM PEAK FOCAL PRESSURE OF THE CARRIER AT 2.65 MHz FOR VARIOUS INPUT VOLTAGES AS DETERMINED BY THE RADIATION FORCE TARGET DEFLECTION CALIBRATION

Voltages (Peak to Peak)	Maximum Peak Focal Pressure (Pa)
4.0	47080
5.0	66580
6.0	81540
7.0	88080
8.0	105300
9.0	115300
10.0	133200
11.0	148900
12.0	166400
13.0	188300
14.0	199700
15.0	215700
16.0	230600
20.0	264200
25.0	339500
30.0	410400

* The data in this table is included in the Easy Reference Table in the Appendix.

through the sample volume. The probe was then removed and the experiment proceeded.

Figure 15 is a full size drawing of a focused transducer and its focal region. This representation emphasizes how small the focal region is for the carrier and receiver. Figure 16 is a similar figure for the exciter. Figure 17 shows the three beam patterns overlayed (not to scale). The intersection of these three regions is the sample volume. The receiver and carrier can be aligned no closer than 55 degrees due to the size of the transducers. The exciter provides full coverage when properly aimed from almost any angle. A value for the sample volume size can be determined for a given minimum acoustic pressure assuming the receiver and carrier foci overlap. The region can be approximately pictured in three dimensions as the intersection of two circular cylinders at an angle of 55 degrees. The radius of the cylinders depends on the acoustic pressure required for the dual frequency method to be effective. In the horizontal plane containing the focus, the area, A_{MAX}, through which a bubble must rise to be in the sample volume is given by

$$A_{MAX} = \frac{4\ r_c\ r_R}{\sin\ \theta} \qquad (30)$$

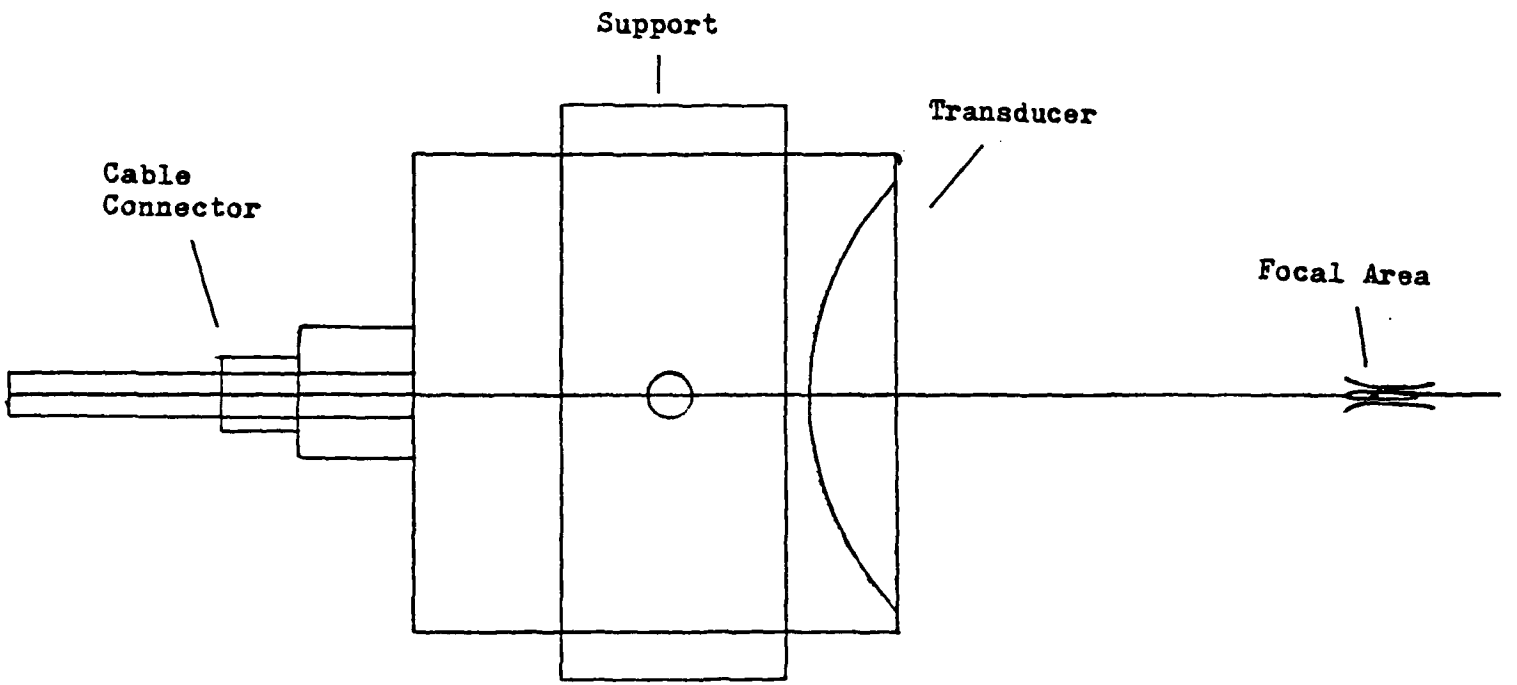

Figure 15 Side View of a Focused Transducer Showing the High Intensity Focal Region (Actual Size)

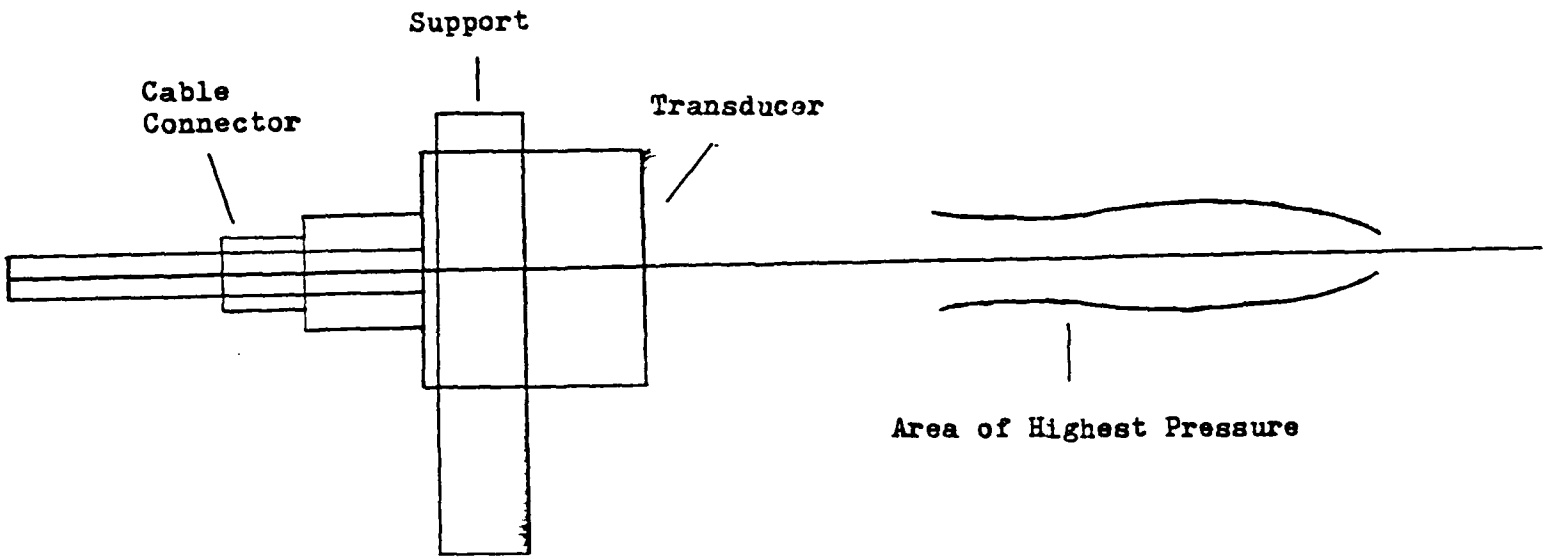

Figure 16 Side View of the Exciter Transducer Showing the High Intensity Portion of the Beam Pattern (Actual Size)

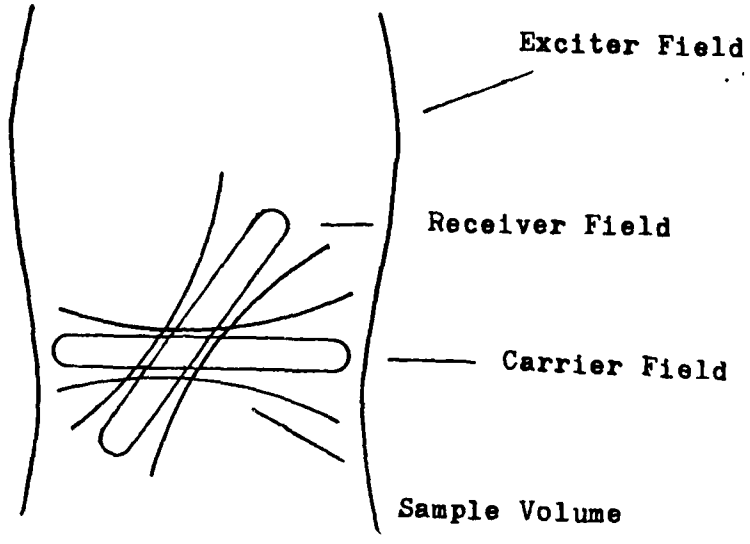

Figure 17 Beam Pattern Intersection

where,

r_c = effective radius of carrier cylinder

r_R = effective radius of receiver cylinder

θ = beam pattern intersection angle

The maximum vertical dimension of the sample volume is the minimum of the diameters of the intersecting cylinders, called H_{MAX}.

These equations were used to calculate the values shown in Table 12. The sample volume is not isobaric. The pressure is maximum in the center. Volumes of decreasing pressure surround the focus much like the skin of an onion. The geometry gets much more complicated farther axially from the focus, especially if the foci are not at the same point.

Using the known sizes and rise velocities of the bubbles, it is possible to determine the length of time a bubble is in the carrier field at a given pressure. It is also important to realize that it is very unlikely that the bubble will pass directly through the focus. Figure 18 is a simplified view of the sample volume cut into volumes of relatively constant pressure. Top and side views are shown. The side view is looking axially toward the carrier. The three dotted lines show single paths by which bubbles may rise through the sample volume. The paths are labeled by the maximum carrier signal pressure encountered. The exciter

TABLE 12 SAMPLE VOLUME SIZE CHARACTERISTICS FOR $\theta = 55°$

CARRIER PRESSURE (dB re MAX)	$r_c = r_r$ (mm)	A_{MAX} (mm^2)	ΔA (mm^2)	H_{MAX} (mm)	ΔH (mm)
0 to -1	0.2	0.20	0.20	0.4	0.4
-1 to -3	0.3	0.44	0.24	0.6	0.2
-3 to -6	0.5	1.22	0.78	1.0	0.4
-6 to -14	0.8	3.13	1.91	1.6	0.6
-14 to -20	1.0	4.88	1.75	2.0	0.4
-20 to -35	1.5	10.99	6.11	3.0	1.0

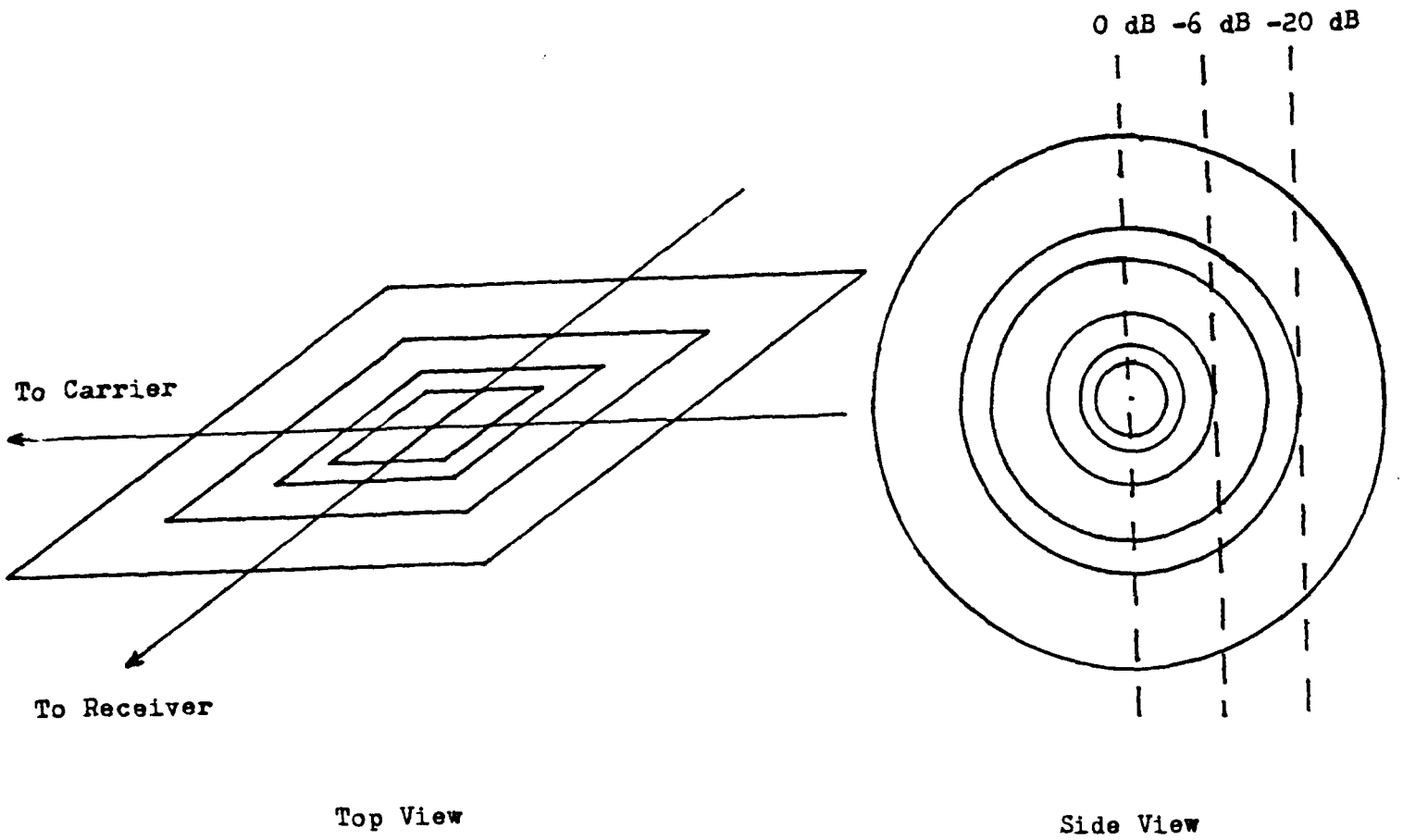

Figure 18 Simplified View of the Sample Volume

field is assumed constant and maximum over this small area. Table 13 depicts the time history of 100 μm, 20μm, and 9 μm bubbles as they rise along these three paths. It is clear that a 30 kHz bubble stays in the sample volume no longer than 0.17 seconds. Though this time is enough for the bubble to be excited it is very short for the receiving equipment to detect the signal. If rise time was the only consideration, then any bubble smaller than 30 μm radius would be in the sample volume at least 1 second. Unfortunately, radiation force of the exciter and carrier push bubbles out of the sample volume. The smaller the bubble, the more it is pushed and less likely to stay in the sample volume. To reduce this effect, the maximum pressure must be reduced. This, in turn, reduces the sample volume further. A compromise must be made.

D. ELECTRONIC EQUIPMENT

This section will detail the primary experimental setup in two major sections, drive signal generation and receiving equipment setup. The total system diagram is shown in Figure 19.

1. Drive Signal Generation

The carrier signal was a 2.65 MHz sine wave. Because the sum and difference signals flank the carrier on a spectral plot, any anomalies near the carrier frequency could not be tolerated. This criterion led to the selection of the HP

TABLE 13 TRAVEL TIME AND CARRIER PRESSURE FOR BUBBLES TRAVELING ALONG THE PATHS SHOWN IN FIGURE 18

BUBBLE	TIME (mSEC) 100 μm	20 μm	9 μm	PATH	PRESSURE (dB re MAX) 0dB	-6 dB	-20 dB
0	0	0		-35↑	--	--	
5	89	434			-35↑	--	
22	398	1939				-35↑	
28	521	2538		-20↑			
31	660	3216			-20↑		
40	729	3552		-14↑			
50	912	4444			-14↑		
57	1042	5077		- 6↑			
68	1250	6091		- 3↑			
74	1354	6598		- 1↑			
85	1563	7616		0*	- 6*	-20*	
96	1771	8629		- 1↓			
102	1875	9136		- 3↓			
113	2083	10150		- 6↓			
120	2213	10783			-14↓		
130	2396	11675		-14↓			
134	2465	12011			-20↓		
142	2604	12688		-20↓			
148	2727	13288				-35↓	
165	3036	14793			-35↓		
170	3125	15288		-35↓			

↑ INCREASING PRESSURE, * MAXIMUM PRESSURE
↓ DECREASING PRESSURE

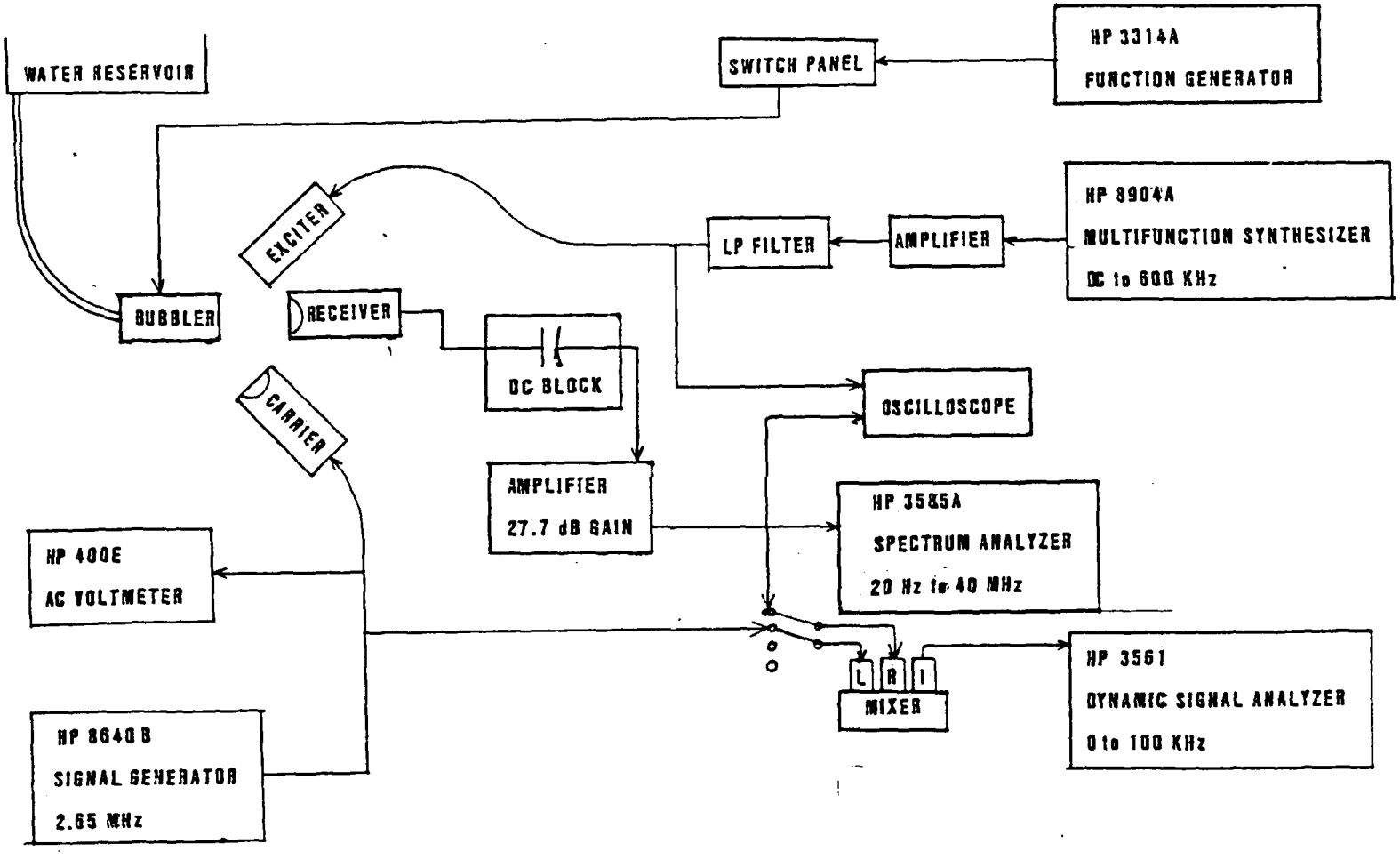

Figure 19 Total System Setup

8640B Signal Generator which has very good spectral purity. C5575 could be driven to provide a maximum focal pressure of about one and a half atmospheres without using an amplifier. The voltage was measured with a HP 400E analog AC voltmeter or the oscilloscope.

The excitation signal was originally generated by a HP 3314A Function Generator in the sweeping mode. This method produced bubble detection in most cases, but proved to be somewhat ambiguous in bubble size estimation. With the sweeping function generator, any given bubble's resonance frequency is broadcast once in the sweep interval. However, by broadcasting band limited white noise every frequency is present (though with randomly fluctuating amplitude), increasing the probability of detection. A HP 8904A Multifunction Synthesizer was used to generate the band limited white noise. An Amplifier Research model 50A15 amplifier with a maximum power of 50 watts and a frequency range of 20 kHz to 15 MHz was used to amplify the noise. A passive low pass RC filter was used to eliminate frequency components above 500 kHz. This signal was monitored periodically on the spectrum analyzer to verify proper frequency coverage. An oscilloscope was used to verify the overall noisy quality of the signal. The exciter was driven at high power to ensure enough energy was present at each frequency to excite any bubble in the size range of interest into large amplitude resonant oscillations.

2. Receiving Equipment

The receiving system consists of a common branch supplying three independent detection devices. The receiving transducer converts acoustic signals to electrical signals. This signal passes through a DC blocking capacitor and an amplifier with a constant gain of 27.7 dB over the range of interest. Three paths diverge from this point. The first goes directly to an oscilloscope. The second into the 1 megaohm input to the HP 3585A Spectrum Analyzer. The third path leads to a HP 3561 Dynamic Signal Analyzer via a frequency mixer. This third path was often disconnected due to certain limitations of the mixer. The functions of these detection devices are discussed in this section and the results chapter.

The HP 3585A Spectrum Analyzer is the heart of the development version of this bubble detector. The oscilloscope was useful, but not capable of yielding quantitative information due to the short duration of the signal and the overwhelming magnitude of the scattered carrier compared to the sum frequency signal. A frequency mixer was employed to take the high frequency sum and difference signals down to base band. Then the HP 3561 Dynamic Signal Analyzer could search the first 100 kHz to detect the larger, faster bubbles. This setup was both useful and frustrating. Neither of these instruments are continuously attentive to all frequencies. Bubbles were missed while these machines were busy with

calculations or searching other frequencies. Methods were hypothesized to correct this, but not implemented. These methods will be discussed with the conclusions.

The oscilloscope would display the real time received signal. Without bubbles in the sample volume, this display was a sine wave at the carrier frequency. During a bubble event, this display would increase dramatically in amplitude as the bubble would scatter the exciter and carrier, as well as, the sum and difference frequencies toward the receiver. A sharp increase in the oscilloscope trace amplitude would be interpreted as a scattering event. It was not possible to tell what type of scatterer caused the event due to the speed of the fluctuation. This was used as an indication that a bubble actually passed through the sample volume.

The HP 3585A uses a frequency sweeping receiver. The receiver is sensitive to a narrow bandwidth that sweeps across the frequency range specified. The fastest sweep time is 0.2 seconds. A constant signal will be recorded each sweep. An intermittent signal is recorded only if the sweep is covering that frequency coincidentally. By adjusting the frequency range to sweep both the sum and difference frequency, each bubble has two chances to be detected each sweep. Hence the frequency range for bubble detection was 2.25 MHz to 3.05 MHz. This permitted detecting bubbles of up to 400 kHz resonance frequency.

The HP 3561 uses a fast Fourier transform (FFT) technique. It records an input signal of at least 4 milliseconds, and then computes and displays the frequency spectrum of that signal via a FFT. It does not record data during the computation. An alternative to this method is to take 40 consecutive records of 4 milliseconds, then analyze and display the whole batch. This method is both better and worse. A greater period of time is covered during the consecutive records, but a greater period is left uncovered during the computations.

The mixer required for the use of the HP 3561 has two distinct disadvantages. First, it distorts the received signal mildly in the region of the sum and difference frequencies as seen on the HP 3585A. Second, its own power limitations limit the power that can be simultaneously supplied to the carrier. Of these two, the distortion is the more serious problem.

E. MODE OF OPERATION

Many experiments were performed during the development of this system. Two major tests comprised the validation of the method to detect and size bubbles. The first involved timing a single bubble as it rose through a known distance. The resonance frequency corresponding to the rise time was then compared with the resonance frequency corresponding to sum and difference frequencies indicated on the HP 3585A. The purpose

of this test was to show that the sum or difference frequencies were being detected correctly, and that the sum or difference frequency gave an accurate and consistent indication of the bubble's resonance frequency.

The other major validation test involved sending a single bubble through the sample volume and comparing the outputs of the HP 3585A, HP 3561 and oscilloscope. This test was designed to show that, at least for bubbles having resonance frequencies less than 100 kHz, the spectrum analyzer gave results consistent with those obtained from the HP 3561 Signal Analyzer. The two analyzers process signals differently. The spectrum analyzer samples a given frequency component only once per sweep. The signal analyzer digitizes a complete window of data and then performs a Fourier transform on that data. In that sense, the signal analyzer processes all frequency components simultaneously.

The two validation tests had one significant limitation. Bubbles smaller than 30 μm radius cannot be easily seen by the naked eye to be timed and the HP 3561 cannot detect bubbles with resonance frequencies greater than 100 kHz. Therefore, resonance frequency determination of bubbles smaller than 30 μm radius (which also have resonance frequencies greater than 100 kHz) cannot be verified by either method. In order to partially validate the system at the higher resonance frequencies, coincidence was used. If a very small radius bubble was detected by the system after the bubble generator

was momentarily energized, but no bubble was seen, then the system would be believed. This is not validation, but it is reasonable extrapolation.

Other tests were performed with multiple bubbles in order to determine the systems response in this situation. Bubbles were readily detected, but the system display saturated quickly. This effect will be explained in the results section.

IV. RESULTS

The results of the tests discussed in the previous section are presented in this chapter. However, a brief discussion of the output display of the spectrum analyzer is presented first. The results of the single bubble detection tests, including data from the rise time resonance frequency verifications, follow. Tests of the dependence of the output signal level on the exciter and carrier pressure levels are then considered. Finally, the results of injecting solid particles into the sound field are discussed.

A. TYPICAL OUTPUT DISPLAY

The HP 3585A is the primary detection device for this system. This spectrum analyzer sweeps its frequency window through the range specified by the operator and displays a graph of amplitude versus frequency. Since the signal from a passing bubble is a fast acting transient phenomena, the most useful display mode for the purposes of this thesis is the "maximum hold" mode. In this mode the current display reflects the highest amplitude that has been present in a given frequency bin since the start of data acquisition. The use of this mode not only results in the display of the maximum signal detected but also the maximum noise.

In order to recognize a bubble detection, the display must be understood. Without bubbles, a small portion of the exciter and carrier signals are detected by the receiver. Figure 20 is a plot of the HP 3585A display of the received signal under this case. Figure 21 is the same display after the mixer has been added to the receiver circuitry. Notice that the mixer has both increased the noise in the frequency range 2.25 MHz to 3.05 MHz and reduced the 2.65 MHz carrier signal. Notice also the clean spectral nature of the carrier and the variations in the exciter level (0 → 400 kHz). The high amplitude signal from 4 to 5 MHz in Figure 21 is higher order modulation of the carrier signal with the received signal. This noise is excusable because it is not in the bubble detection frequency range.

In order to detect rapidly rising bubbles, the fastest sweep over the frequency region of interest was needed. This resulted in the 800 kHz span centered at 2.65 MHz being covered in a sweep time of 0.2 seconds. Any bubble with resonance frequency, f_R, in the range 30 to 400 kHz would have both a sum (2.65 MHz + f_R) and difference (2.65 MHz - f_R) in this frequency band. Figure 22 shows the display of this region as it appears without bubbles (and without the mixer). Figure 23 shows the same frequency span after copious bubbles were allowed to rise through the sample volume for five minutes. A comparison of the two figures shows that the carrier level is at least 27 dB higher in Figure 23,

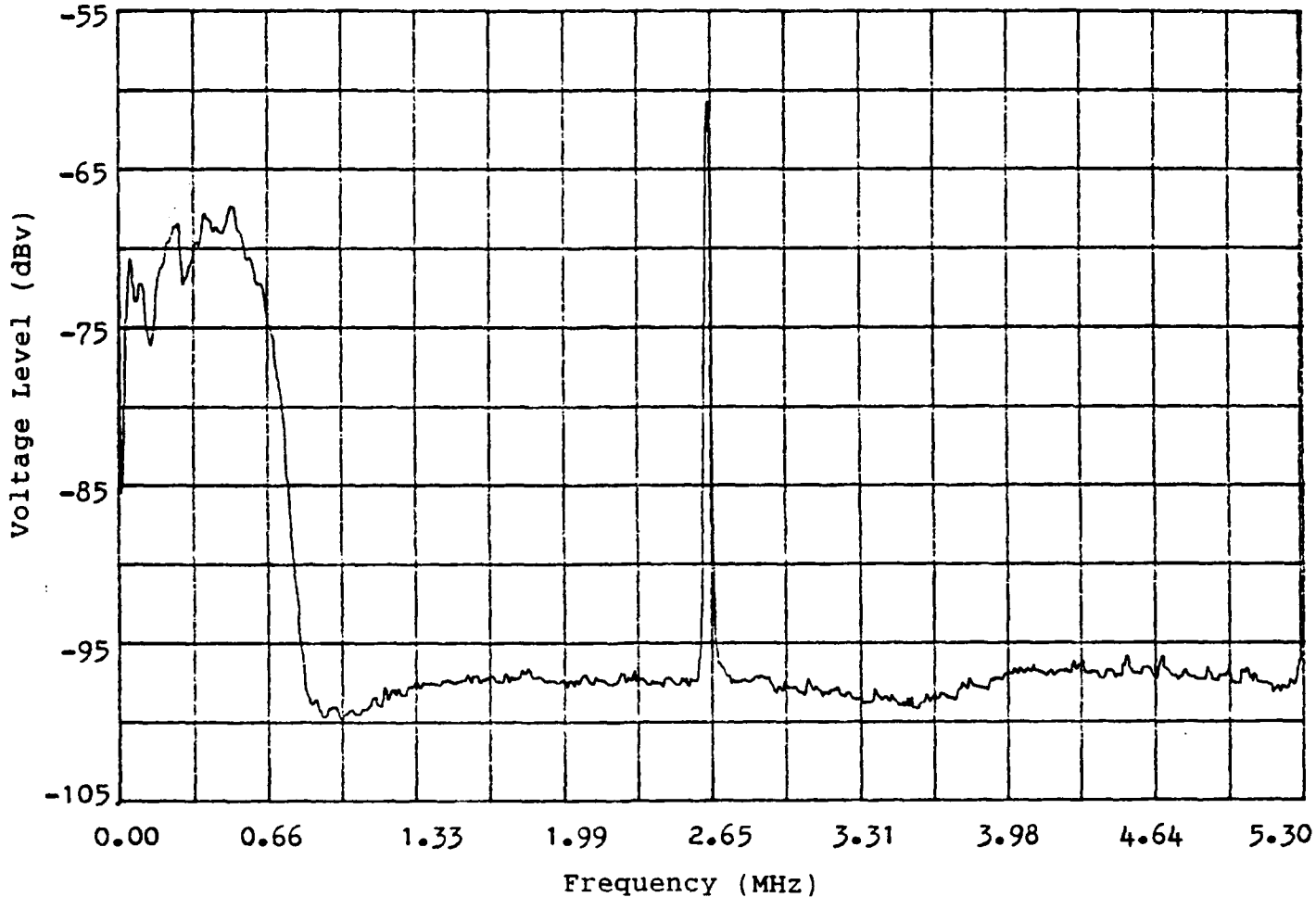

Figure 20 HP 3585A Display without Bubbles, Mixer Disconnected

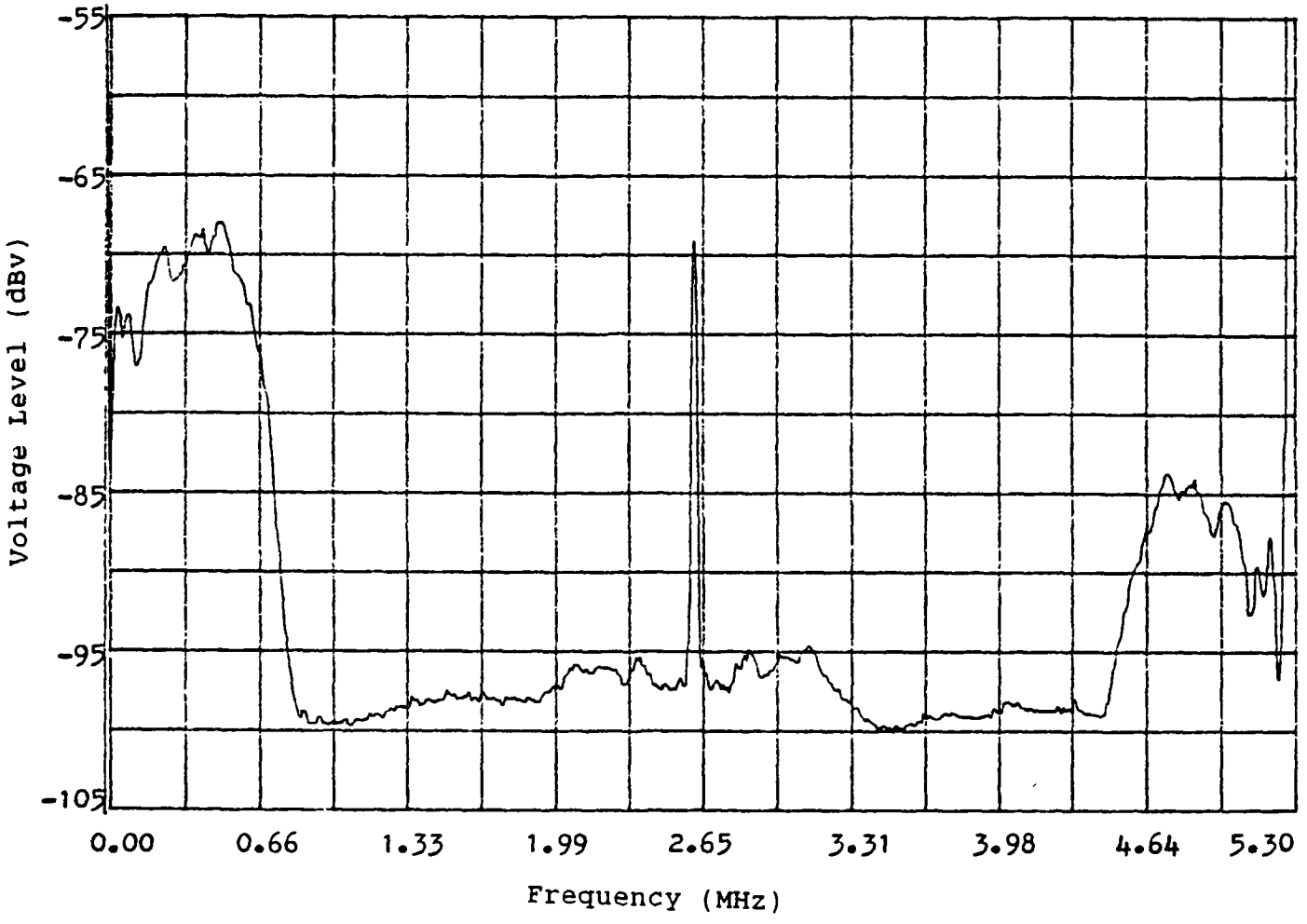

Figure 21 HP 3585A Display with Mixer Connected, No Bubbles

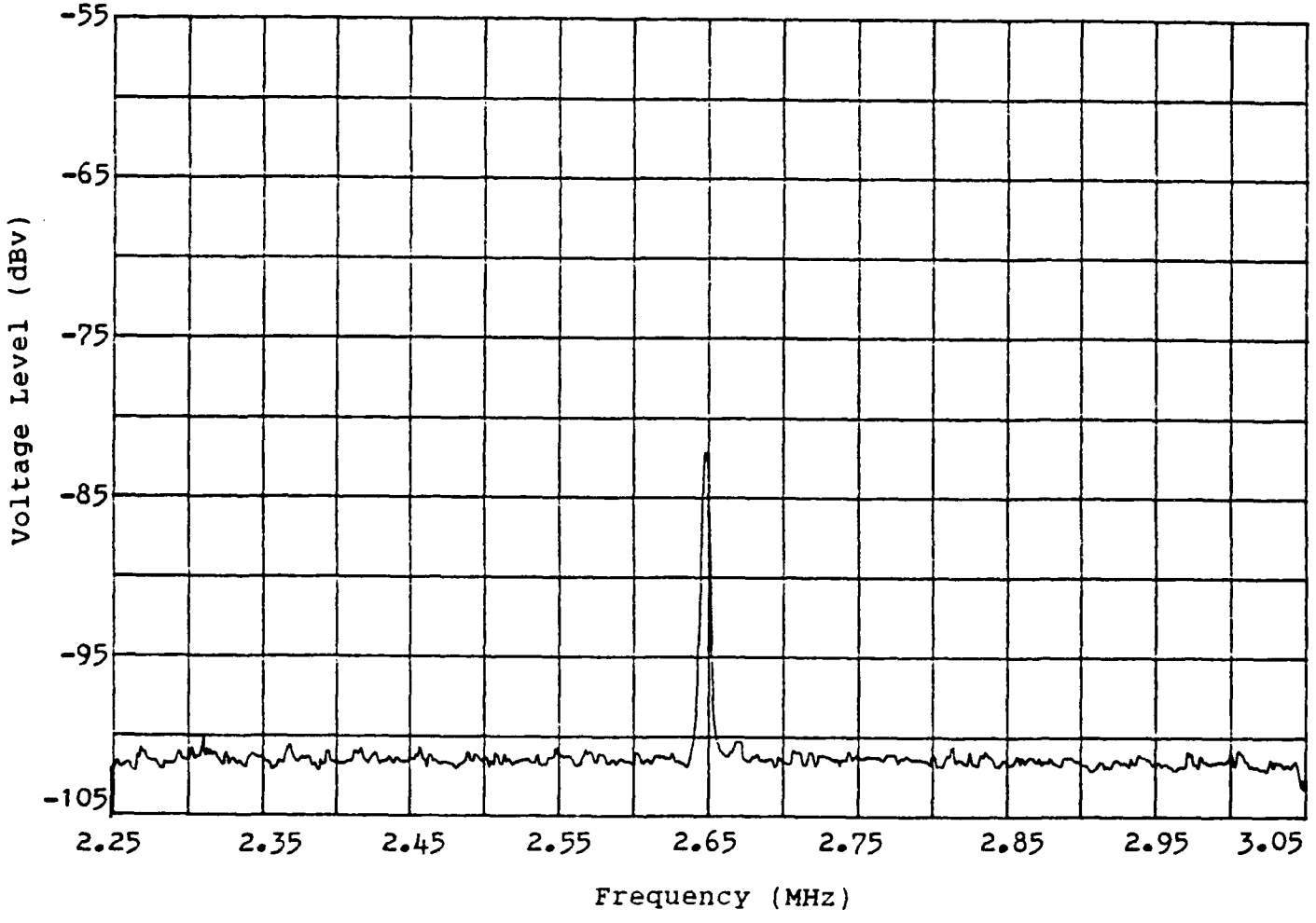

Figure 22 HP 3585A Display of the Detection Band, without Bubbles, Mixer Disconnected (Carrier Focal Pressure = 5070 Pa, Exciter at Maximum Power

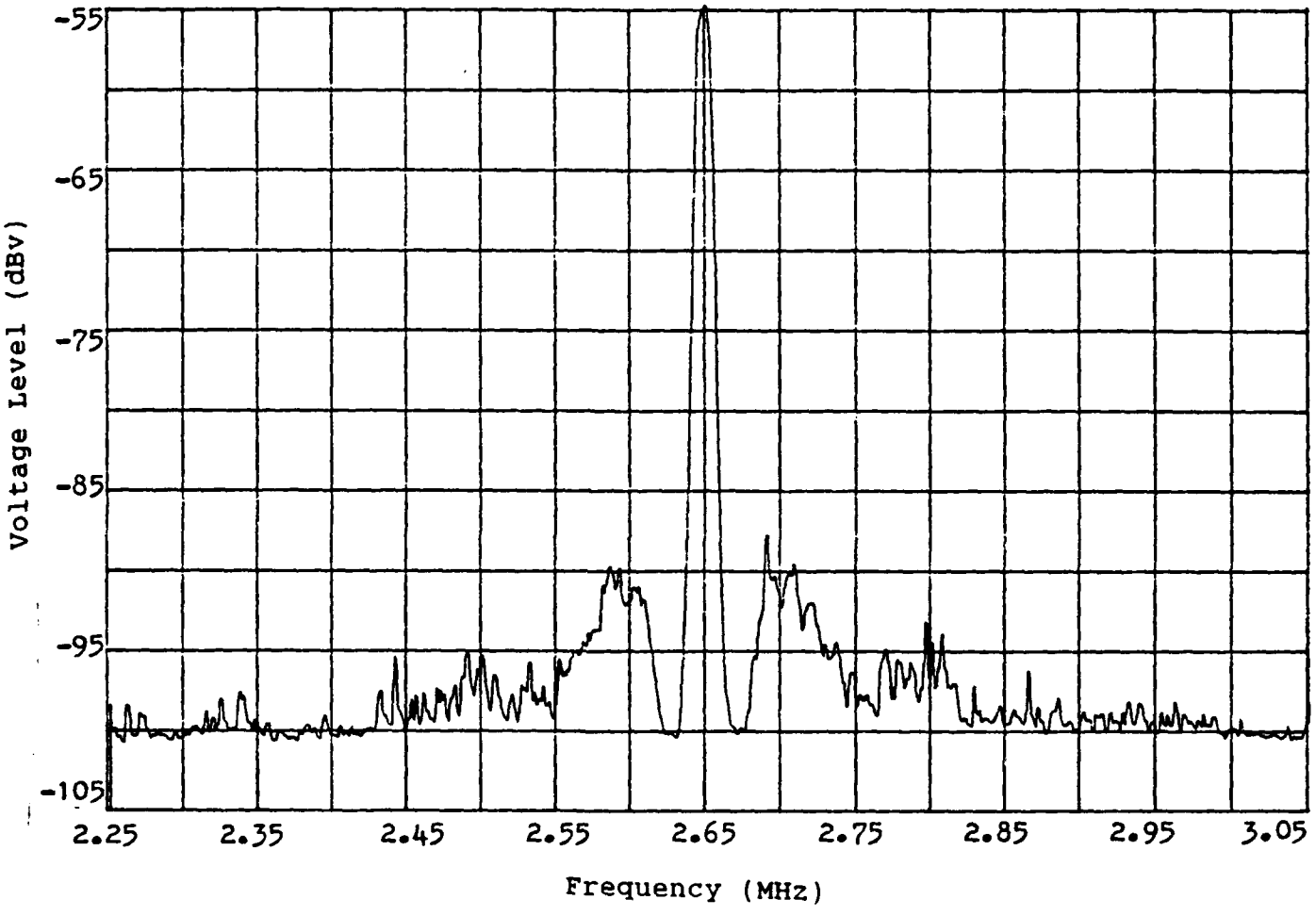

Figure 23 HP 3585A Detection Band Display with Bubbles, Mixer Disconnected (Carrier Focal Pressure = 5070 Pa, Exciter at Maximum Power)

indicating that it was scattered significantly towards the receiver by the bubbles. Sum and difference frequencies were recorded for many bubbles of various sizes with a signal to noise ratio approaching 15 dB. Figure 24 is a superposition of the same type of plots for a higher carrier pressure. The bottom curve is without bubbles and without the mixer. The top curve is with bubbles but not the mixer. The middle curve has both bubbles and the mixer. As shown by the top curve, sum and difference frequencies are detected with a 10 to 20 dB signal to noise ratio. These results are strong evidence which support the bubble detection goal.

Figures 23 and 24 also illustrate system saturation. When the spectrum analyzer is in the maximum hold mode, the signature of a bubble, once detected, is maintained on the display. This signal is now noise to future detections and the system becomes less sensitive to bubbles of size similar to those it has already detected. This saturation effect is not a problem for these experiments since they involved only one bubble at a time. However, it indicates that this processing arrangement is not well suited for multiple detections.

B. SINGLE BUBBLE DETECTION AND RESONANCE FREQUENCY DETERMINATION

Figures 25, 26 and 27 show three variations of single bubble detection and resonance frequency determination. In each case, both the sum and difference frequencies were

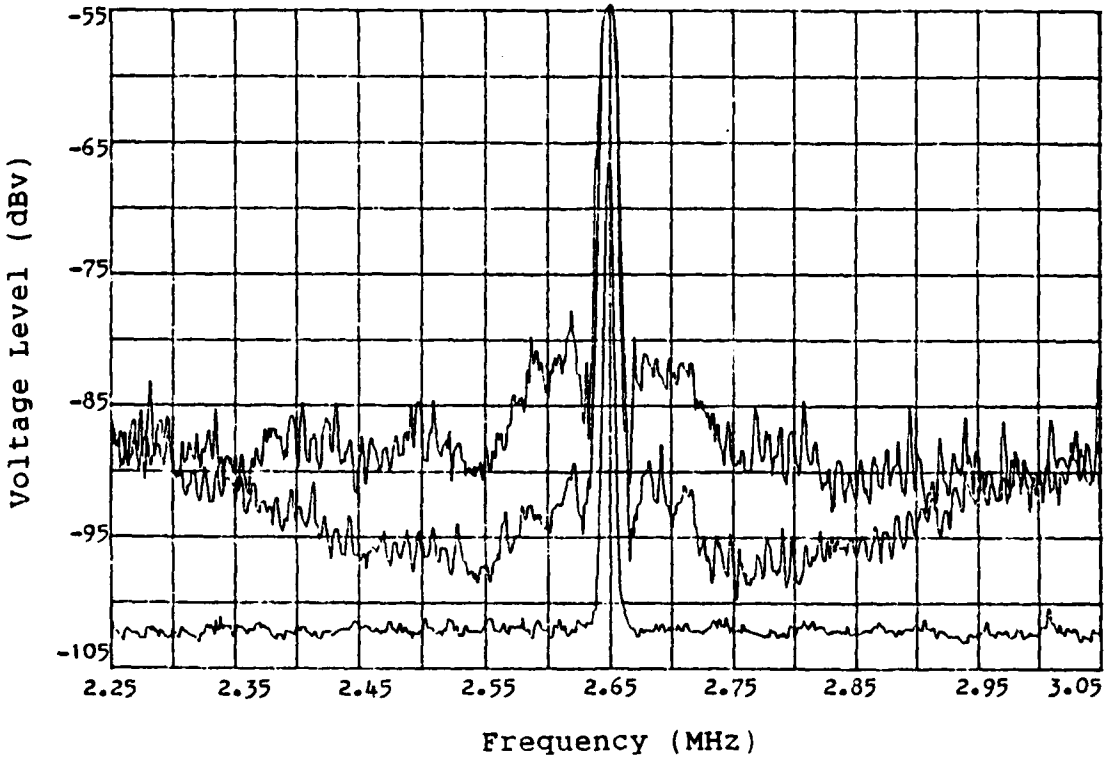

Figure 24 Superposition of Three HP 3585A Detection Band Displays

bubbles	Mixer	Carrier Focal Pressure	Exciter Pressure
Top: Yes	Disconnected	26800 Pa	Maximum
Middle: Yes	Connected	12800 Pa	Maximum
Bottom: No	Disconnected	26800 Pa	Maximum

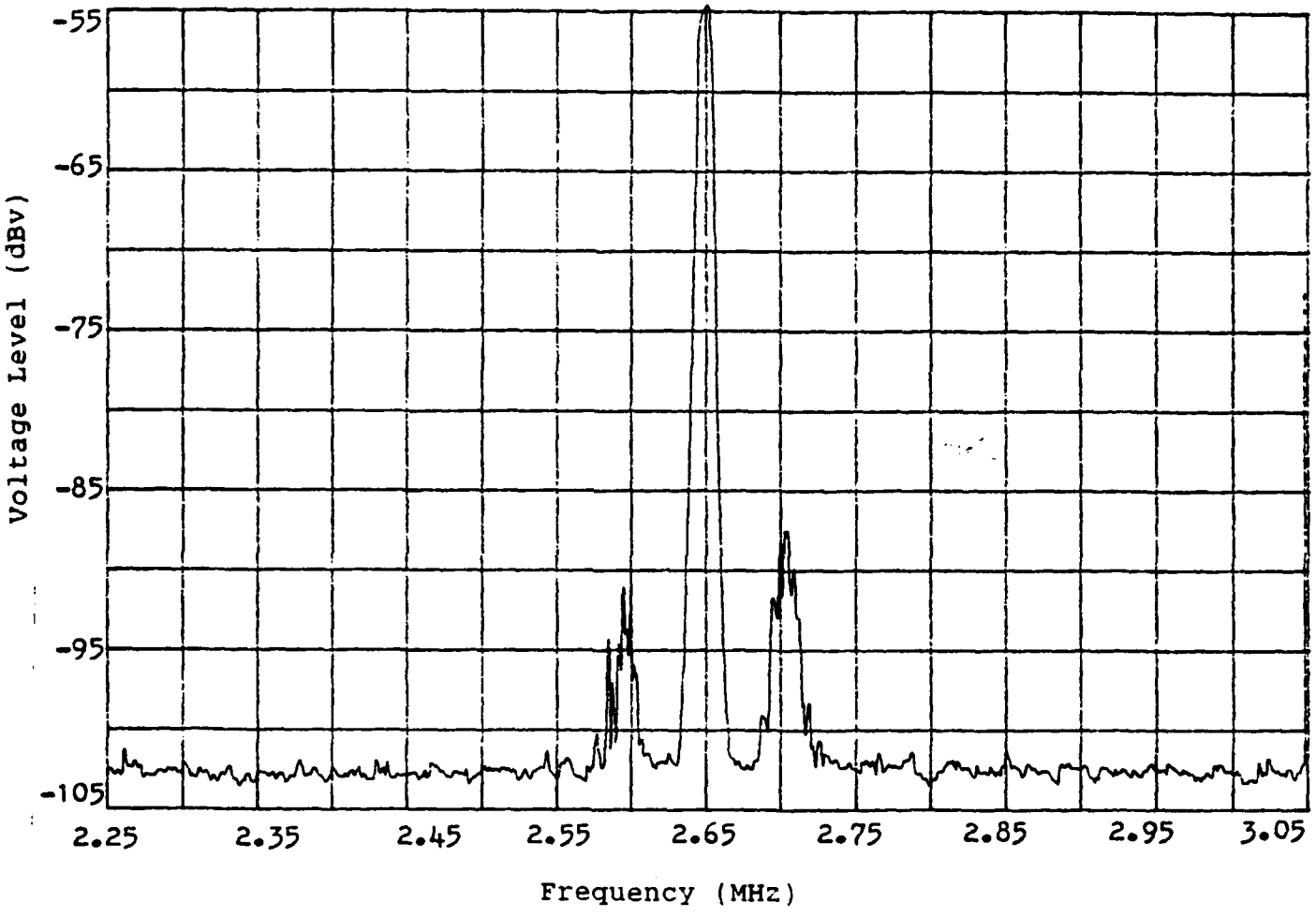

Figure 25 Detection and Resonance Frequency Determination of a 55.3 kHz (by Rise Time) bubble. Peak Signal is at 56 Khz. Carrier Focal Pressure = 102400 Pa, Exciter at Maximum Power

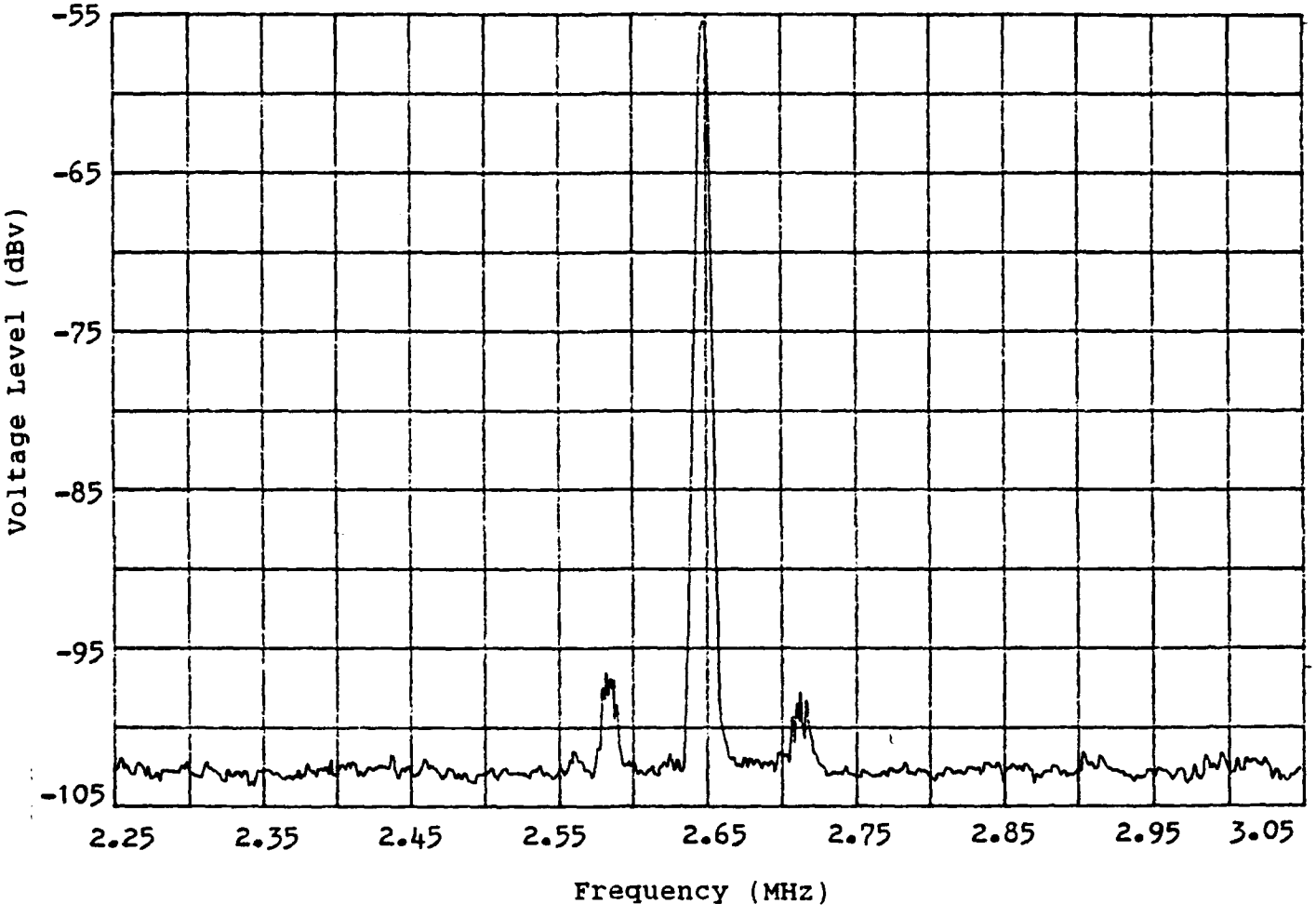

Figure 26 Detection and Resonance Frequency Determination of a 62.4 KHz (by Rise Time) Bubble. Peak Signal is at 65.6 kHz. Carrier Focal Pressure = 102400 Pa, Exciter at Maximum Power

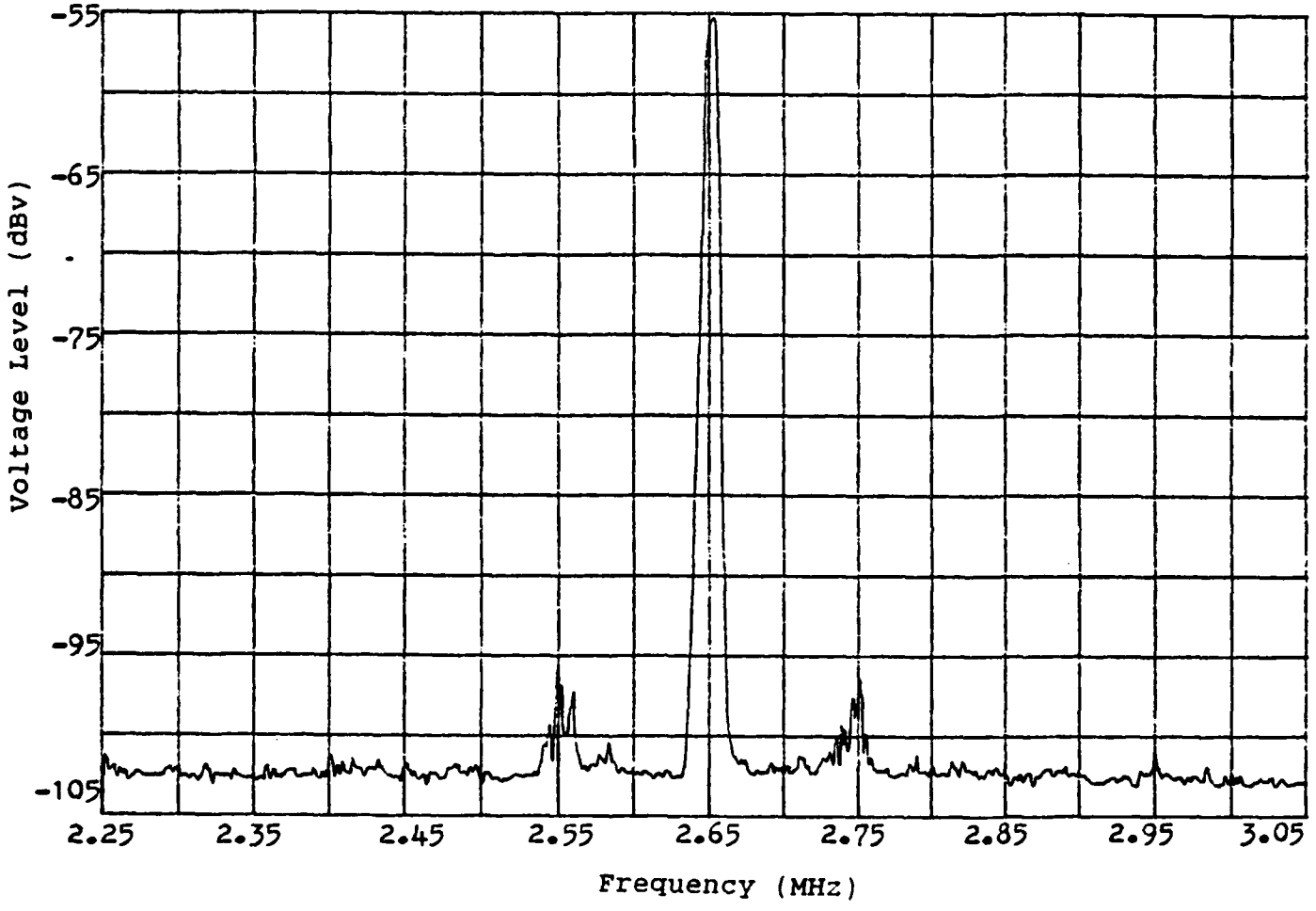

Figure 27 Detection and Resonance Frequency Determination of a Bubble too small to verify with the rise time method. Peak signal is at 100 kHz. Carrier Focal Pressure = 102400 Pa, Exciter at Maximum Power

detected. Notice that the signal to noise level is a little different in each case. This difference is most likely due to the wide variety of carrier pressure available in the sample volume.

The frequency of highest amplitude, other than the carrier, corresponds to the bubble's resonance frequency. Using the rise time method to independently determine resonance frequency verified the accuracy of the frequency determination. A large number of such comparisons were made. Figure 28 shows the agreement between the two methods. Perfect agreement would correspond to all of the data points falling on the line having a slope equal to one. The two methods agree to within a few kilohertz in most cases. A major source of error lies in timing the tiny rising bubbles.

While performing these single bubble experiments it was noted that not every bubble was detected. There were some cases where bubbles passed through the sample volume sufficiently to show a transient on the oscilloscope but did not result in sum or difference frequency peaks on the HP 3585A display. Since the oscilloscope verified the presence of a received signal, the HP 3585A was apparently inattentive to the frequencies of interest. The absence of these frequency peaks could have been due to: (1) the HP 3585A performing an internal calibration procedure that prohibited sampling while the bubble was in the sample volume, (2) the HP 3585A sweeping the wrong frequencies during a fast bubble

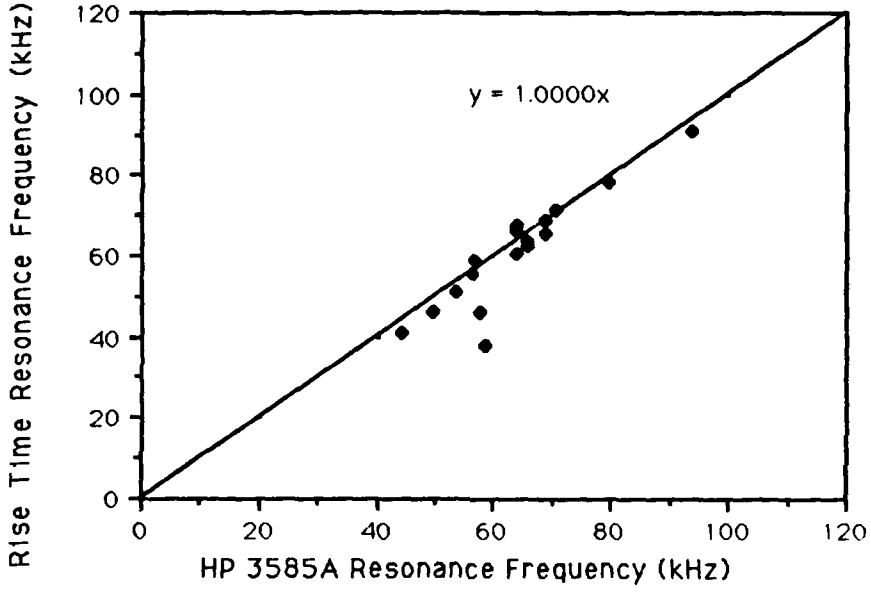

Figure 28 Resonance Frequency Comparison
Rise Time versus HP 3585A

transient, (3) the bubble passing through a portion of the sample volume having too low a signal to noise level to permit detection, and (4) too much energy being scattered into the receiver causing the HP 3585A to overload. Some credence is given to all of these possiblities. Some displays would detect the sum or difference frequency but not both. Only alternative number (2) above makes sense in this case, since both signals should be present in approximately the same magnitude at the same time.

The HP 3561 uses an FFT technique to analyze the spectral nature of the signal. However, the use of this instrument did not improve the probability of detection for several reasons. First, there is significant time over which the instrument is not sampling during computations, calibration and display. Second, the instrument's frequency range is limited to 0 to 100 kHz. Hence, it could never detect a 100 to 400 kHz bubble. Finally, it requires use of the mixer which inherently lowers the signal to noise ratio. Some low power detections might be lost in the noise.

However, the HP 3561 was useful. First, it verified that FFT techniques can be employed in this problem. Second, it provided a different method to verify the accuracy of the resonance frequency determination. Figure 29 shows the display of the HP 3561 for the case without bubbles. This shows the noise floor as a function of frequency. Since the mixer demodulates the signal from a 2.65 MHz carrier, the

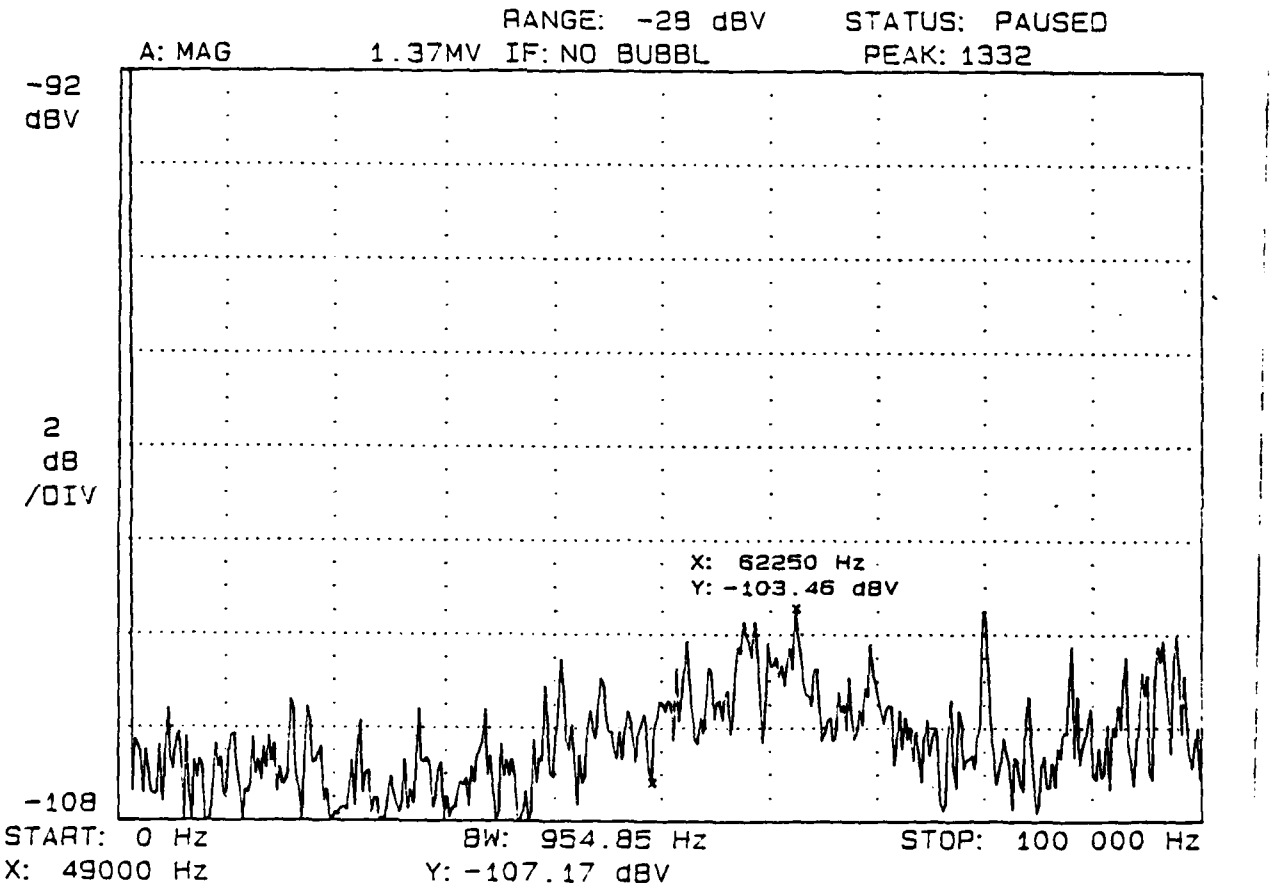

Figure 29 HP 3561 Display without Bubbles

frequency scale labeled 0 Hz to 100 kHz actually represents 2.65 to 2.75 MHz.

Figure 30 shows the detection and resonance frequency determination of a single bubble by the HP 3561. Using the time buffer mode, the HP 3561 continuously recorded 40 data records prior to processing. Ten of these data records were analyzed and plotted here. The first three and last six of the ten records show no hint of a bubble. Record four, on the other hand, strongly indicates the presence of a 40.25 kHz bubble. This figure indicates the transient nature of the bubble signals. The HP 3585A simultaneously detected the same bubble. Figure 31 is a copy of the HP 3585A display for this run. It shows the difference frequency strongly at 2.61 MHz, which represents a resonance frequency of 40.00 kHz. The sum frequency did not show up due to the high speed of this buble transient. In other words, the signal was gone before the 20 milliseconds needed for the sweep to advance to the sum frequency had elapsed. The HP 3561 bears this out since each record represents only 4 milliseconds of data. Although two peaks of approximately the same amplitude are shown in Figure 30 the one at 40.25 kHz is actually much larger. It appears to be the same amplitude because, it exceeded the maximum scale and was truncated. The level -87.13 dBV is, however, accurate.

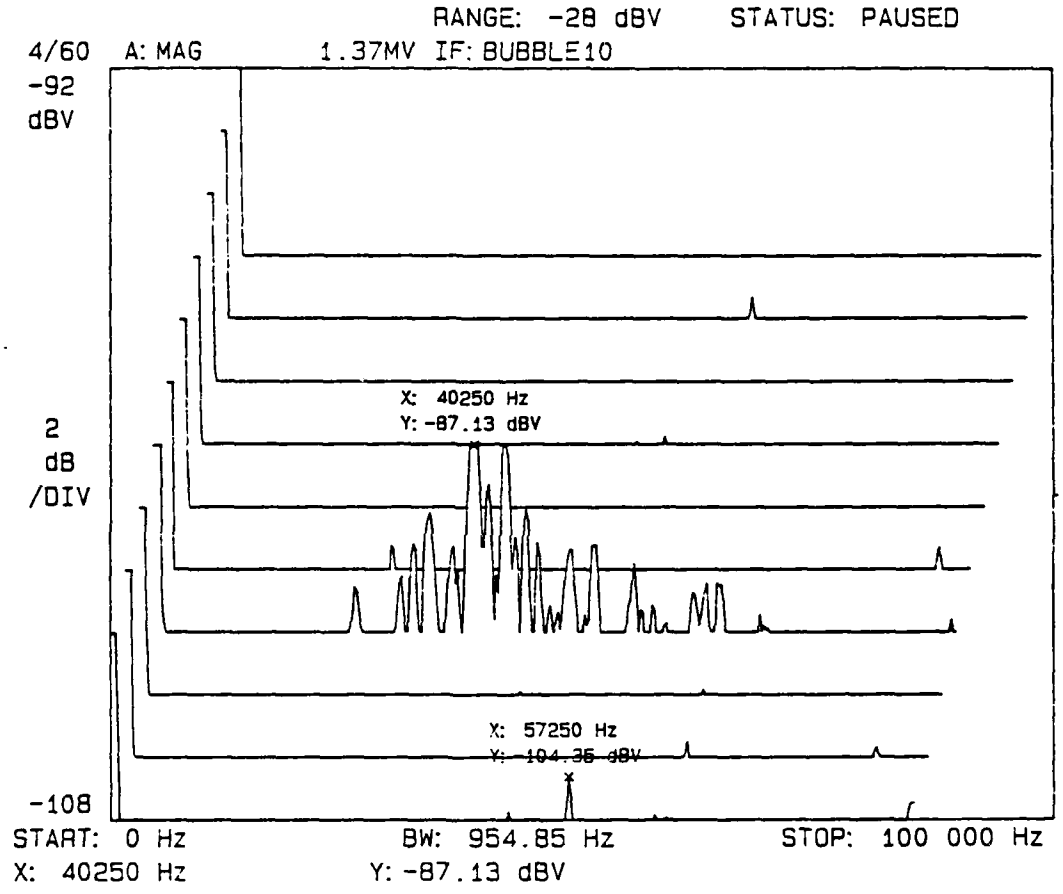

Figure 30 HP 3561 Display of 10 Data Records' Frequency Content. The Fourth Trace Shows a 40.25 kHz Bubble Detection.

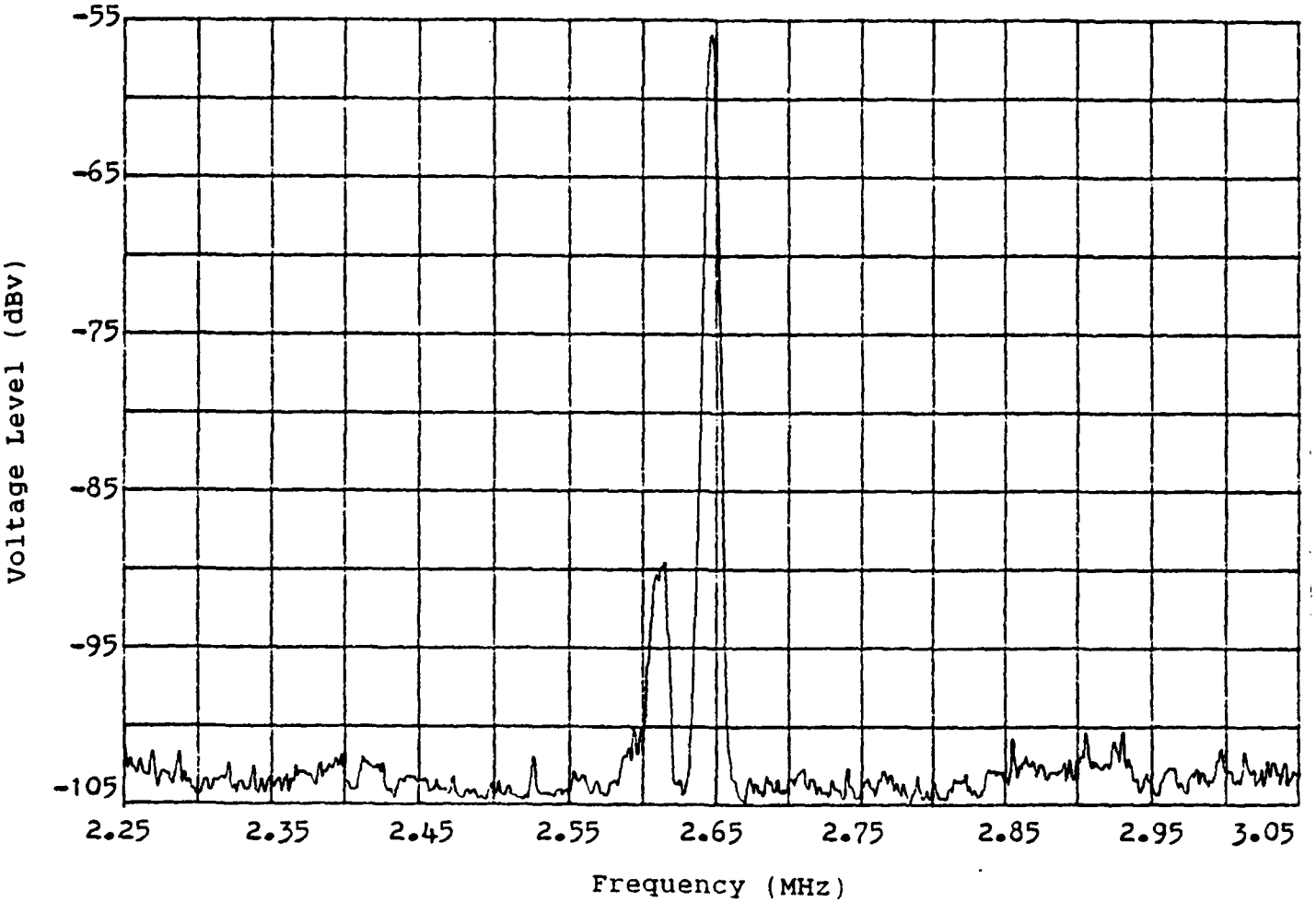

Figure 31 HP 3585A Display Showing Detection of the Same bubble as Figure 30. Peak Signal is at 40.0 kHz.

C. VERIFICATION OF DUAL FREQUENCY METHOD PRESSURE DEPENDENCIES

In order to confirm that the detected signals are in fact produced by the mechanism described by the dual frequency method, the peak pressure amplitudes of the detected signals were compared to the predictions of equation 2. The calculations were performed for many different bubble sizes using the transducer calibrations to determine the maximum carrier pressure, the exciter pressure at the bubble resonance frequency and the pressure amplitude of the sum or difference frequency. Figure 32 is a comparison of the actual received level and maximum calculated sum or difference pressure at the receiver face divided by the product of carrier and exciter pressure. The expected values were given earlier in Table 4. None of the actual values exceeded the maximum expected values. The lower actual values are attributable to the fact that most bubbles encountered less than maximum carrier pressure.

According to the theory of dual frequency bubble detection, the amplitude of the return signal depends on the pressure amplitudes of the carrier and excitation at the location of the bubble. In order to get an idea of what drive pressures were required, the exciter pressure was varied over a range of 7.36 dB with a constant carrier pressure amplitude of 102 kPa. Since the carrier pressure varies dramatically over short distances and the excitation pressure varies wildly with frequency, it would take an enormous amount of data to

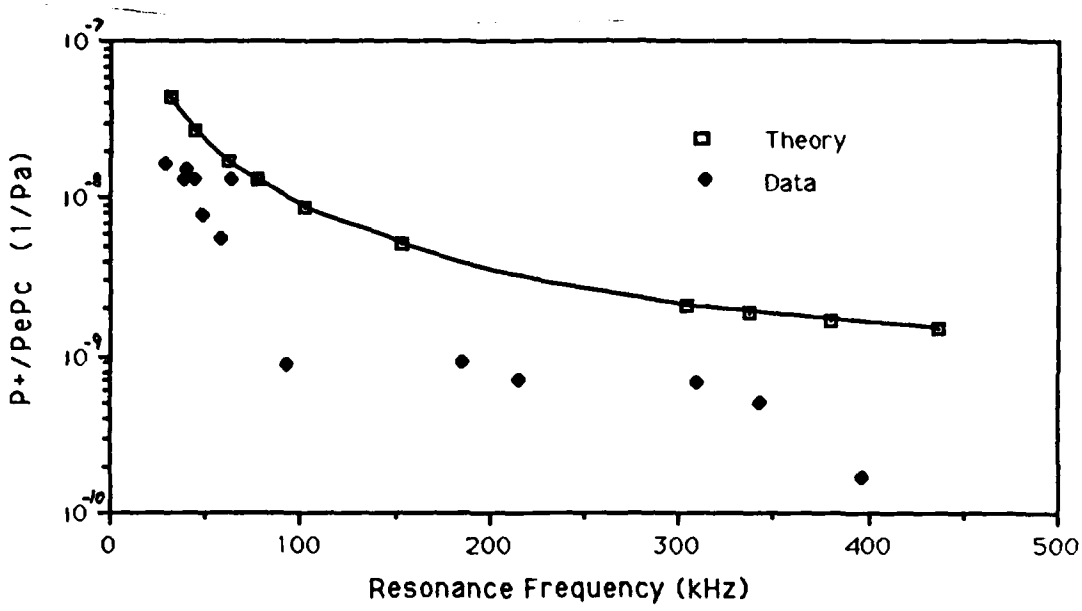

Figure 32 Comparison of Actual Pressure Relationship with Maximum Expected

verify equation 2 with this implementation. In spite of this, Figure 33 shows that the signal level varies with the exciter pressure. The exciter pressure is lowest for frequencies of about 140 kHz. Therefore, 140 kHz bubbles are detected with the weakest signal. The main reason for the curves not being flat is the variations of excitation pressure with frequency. Another factor is that smaller bubbles naturally have smaller signals for the same excitation.

Figure 34 shows a similar family of curves. This time the exciter was held constant at the maximum value. The carrier pressure was varied by a factor of 2 (6dB). Again, the bubble signal decreased as carrier pressure decreased. It is clear that for better signal to noise ratios, the carrier and exciter pressures should be as high as possible.

D. DISCRIMINATION OF BUBBLES FROM SOLID PARTICLES

Dry grains of sand, ranging in size from 1 μm to 1 mm diameter were dropped into the water over the sample region. The grains rarely entered the sample volume, but when one did it almost always produced a signal similar to that produced by bubbles. These signals were attributed to the presence of entrained gas pockets, some of which were visible, on the dry sand. It was reasoned that wet sand would not produce the same type of signals. Therefore, pre-wetted sand was more carefully injected into the sample volume. Only occasionally would an extraneous bubble indication be noted under these

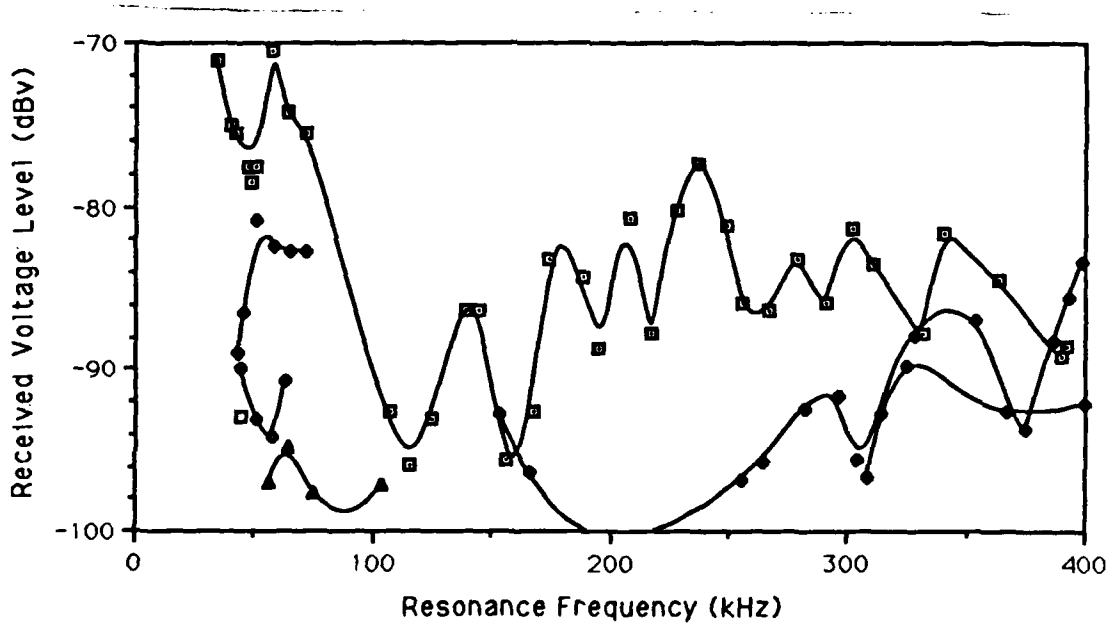

Figure 33 Received Signal Variations with Changing Exciter Pressure

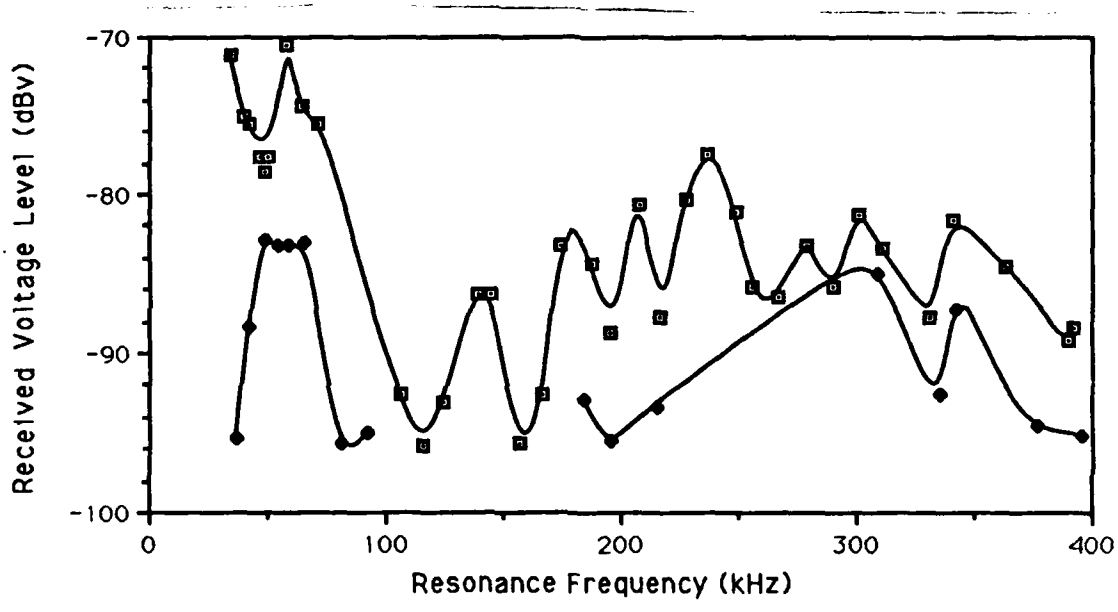

Figure 34 Received Signal Variation with Changing Carrier Pressure

circumstances. This was thought to be due to an infrequent gas bubble in the slurry. The most common response of the system to a solid is an increase in the received carrier and exciter signals. As long as the pressure of these signals is less than that required for medium non-linearities, such as the parametric effect, no sum or difference frequencies should be detected.

Hollow glass beads were also injected into the sample volume. The response was identical to that for gas bubbles. This response semed reasonable since the glass beads were at least 90 percent gas by volume. They floated rapidly to the surface. The results of these measurements indicate that the dual frequency method is capable of detecting bubbles as well as other partially gaseous matter. However, it is insensitive to non-gaseous scatterers.

E. DISCUSSION

Up to this point, many facts and figures have been presented, but the full implications have not been discussed. This section will review the evidence presented for this implementation of the dual frequency method for detecting and sizing bubbles.

The first requirement was to detect bubbles. This goal clearly was accomplished. Bubbles were detected through the range of interest, though the majority of the events were less than 100 kHz. Data to support this was taken with single

bubbles and lots of bubbles, free rising bubbles and convected bubbles, varied excitation and carrier pressure levels. By doing this, not only were bubbles detected, but some limitations of bubble detectability were discovered. These will be highlighted later in this section.

The ability to directly determine the resonance frequency of a bubble has been shown. Two independent signal processors were used to show that this technique was not based on a peculiarity of one type of processor. The resonance frequency determination follows the simple rule that the bubble has its maximum response at resonance. Therefore, the maximum received signal in the detection band corresponds to the resonance frequency. The rise time method of resonance frequency estimation supported the dual frequency method results. The agreement in the results of the two processors and the rise time method was best when detected with high signal to noise. This was not surprising since low signal to noise was often due to poor bubble signal timing with respect to the frequency sweep for the HP 3585A or the signal data record for the HP 3561. Strong signal to noise indicated that the bubble was properly detected while in the processor's analysis window. In these cases, this dual frequency method determines the resonance frequency to within the signal processor's analysis error.

The tests with solid particles indicated that this method can determine the resonance frequency of solid borne or

membrane enclosed gas volumes. The accuracy of these measurements has not been shown, but the presence of a signal very similar to that of a pure bubble for these gas volumes with solids suggests the same ability to correctly determine resonance frequencies. A solid particle without gas was shown to lack the sum and difference frequency signals. Therefore non-gaseous scatterers are easily distinguishable from various types of gaseous scatterers having resonance frequencies in the range of interest. This natural ability to classify a bubble by its acoustic resonance parameters has far reaching implications for the study of bubbles in both clean and dirty environments.

During the bubble experiments, a wide variety of signal to noise levels were noted. Some bubbles transited the sample volume without any indication of its presence on the processor's display. Others were detected with more than 20 dB of signal to noise. Much of this was probabilistic since the bubble's path through the sample volume and signal timing to the signal processor were not controllable. This random positioning and timing meant that any single run with any single bubble could not be directly related to other runs. To compare one test setup with another many data runs were taken. The maximum signal to noise cases were considered to have had the most optimal sample volume positioning and timing. Thus, the differences between these runs would be due to the actual parameter changes between test setups. An

example of a test setup change is the exciter pressure variations previously discussed and shown in Figure 33. To verify the relationship of bubble signal pressure to exciter pressure many bubble runs were made at each pressure. The maximum bubble signal at each pressure was considered to be optimum in position and timing.

The sum frequency pressure relationship given by equation 2 was tested by doing these comparisons. To establish a threshold of detection the whole system must be understood. For this system, the detection band noise level was about -100 dBv. To obtain 10 dB signal to noise, a signal of -90 dBv is needed at the instrument. Subtracting the 27.7 dB amplifier gain yields a necessary -117.7 dBv out of the receiver. It is easy to calculate the pressure required at the receiver face to generate this voltage. Using equation 2, the required excitation pressure can be found for each frequency given the carrier pressure. Table 14 shows the results of these calculations.

The pressure produced by the exciter was well above the calculated values of Table 14. The carrier pressure was also higher than the value assumed for this table. These higher pressures produced the data with 20 dB signal to noise. The weaker signals were due to the losses induced by poor positioning and timing. The numbers in Table 14 are valid for any system since they are simply pressure relationships. The

TABLE 14 EXCITER PRESSURE REQUIRED FOR 10 dB SIGNAL TO NOISE GIVEN r = 7.7 cm, CARRIER PRESSURE = 3 X 10^4 Pa

FREQ. (MHz)	P_t at Receiver for -117.7 dBv (Pa(peak))	Exciter Pressure (Pa(peak))	FREQ. (kHz)
2.70	0.0197	29.6	50
2.75	0.0194	68.0	100
2.80	0.0195	115	150
2.85	0.0191	184	200
2.90	0.0191	254	250
2.95	0.0190	274	300
3.00	0.0189	319	350
3.05	0.0190	374	400

receiver output voltage would, of course, vary with different receivers. This makes this analysis specific to this system.

If a system could be designed to produce these exciter and carrier pressures and receiver coverage over a broad sample volume, it would detect all bubbles with about 10 dB signal to noise ratio. This assumes that a larger sample volume would alleviate the critical timing problem since the bubble would remain in the sample volume longer.

V. CONCLUSIONS

The goals of this bubble detection system have been accomplished. The system has demonstrated the ability to detect bubbles with resonance frequencies from 30 to 400 kHz when they entered the sample volume. The resonance frequencies of these bubbles were accurately determined by the system. The ability to distinguish between bubbles and non-gaseous particles was shown. Parameters for creating a system with a high probability of bubble detection were accumulated. The ability to determine the resonance frequency of scatterers containing a small gas volume was also noted.

With the achievement of these goals, the dual frequency method for bubble detection and resonance frequency determination becomes a powerful tool. It can be used to analyze bubble populations or to study the dynamics of single bubbles under the influence of stress. Studies may be done using this technique to study the effect of varying a fluid's viscosity or surface tension on a bubbles damping constant. There are a number of areas for application of this technique. The next section recommends items to consider to improve the performance of a dual frequency method bubble detector.

A. RECOMMENDED IMPROVEMENTS FOR A CONTINUOUS BUBBLE DETECTION SYSTEM

Many items have been mentioned that effect the chances of detecting a bubble with this system. Some improvements must be made to achieve an ideal system. Here is a summary of areas of concern.

	Concerns
* Sample Volume	- too small - too variable - too weak
* Bubble	- path and time in sample volume
* Receiving Equipment	- needs to sample continuously - needs large dynamic range (to detect small sum and difference frequency signals in the presence of large scattered carrier and exciter signals) - data output management
* Environment	- noise level in detection band - number of bubbles: saturation effect and signal extinction - vibrations: disturb sample volume alignment - flow rate: speed of bubble through sample volume - quantity of suspended solid scatterers

1. Sample Volume Related Improvements

A bubble must pass through the sample volume to be detected. A large sample volume permits easier coverage of reasonable volumes. The smaller the sample volume is with respect to the total system, the lower the probability of

detection. The implementation tested here had virtually the smallest possible sample volume.

Variations in the carrier and excitation pressures and receiver efficiency within the sample volume allow for highly variable received signals when a bubble is present. If the lowest possible received signal is less than the noise, detection opportunities will be missed. Driving the exciter with band limited noise in the frequency range of interest provides broad frequency coverage, with only minor temporal variations. The drive current and exciter source strength are functions of frequency. The drive current should be manipulated to excite bubbles equitably, to give each size bubble the energy to obtain the same signal to noise.

The receiver's efficiency may vary with frequency and bubble location. These variations are strictly functions of the transducer. The transducer should be designed or selected to minimize these variations in the frequency range and spatial region of interest. The carrier transducer is monofrequency. Hence, only stability of output power and beam pattern are of concern. The overall goal is to obtain a good sized volume of constant and adequate, but not excessive, acoustic pressure. If this is accomplished, many of the problems associated with a small sample volume disappear.

2. Bubble Related Concerns

The path of travel varies from bubble to bubble, due to a variety of forces acting on the bubble. Gravity, buoyancy, drag and radiation forces are the key players. Of these, radiation force may be the worst. This acoustic phenomena pushes the bubble when the acoustic pressure is high. The resulting motion drives the bubble toward regions of lower carrier and excitation pressure. Keeping the pressure just below the level that causes significant motion is important to solving this problem. Having a relatively large sample volume would help regardless of the cause of the bubbles motion.

The amount of time a bubble spends in the sample volume impacts its detectability. It is a function of the sample volume, bubble speed and path. These items need to be manipulated to achieve an ideal length of time in the sample volume. Too little time results in missed detections. Too much time will limit the rate at which the system can distinguish between individual bubbles.

3. Receiving Equipment Improvements

The receiver must be alert to detect an event. The equipment assembled for this experiment was useful, but not ideal for the job. The received signal needs to be continuously monitored over the frequency range of interest. Only the sum or difference band is actually needed, but both may be wanted for verification. The data needs to be

presented in a format in which new detections are not effected by previous ones. A continuous hard copy spectrogram is a good way to handle large amounts of data.

During a bubble detection, many frequency signals are received. Unfortunately, those of the most interest are of low level. Large dynamic range is needed in the receiver. This allows it to measure the low level signals without overloading due to the high level scattered signals. Filtering the return signal can help this problem. Band pass filtering to accept only the detection band followed by notch filtering to eliminate the carrier would eliminate the unwanted signals' overbearance.

Correcting the overall alertness and relative dynamic range of the receiving equipment would be a major improvement in this system. This would require a system designed for this purpose. Most off the shelf equipment does not have the frequency range or data volume capability needed for a true bubble detection system.

4. Environment Related Concerns

The environment of the test apparatus has a large impact on its effectiveness. Vibrations change the bubbles path, as well as, the sample volume alignment. The quantity of scatterers throttles the amount of power available to excite a bubble and effects the propagation of the bubble's signal to the receiver. The ambient noise in the detection band is a factor in detectability. The environment was not

a major problem in this laboratory experiment. It has the possibility of causing problems, but they are minor compared to the previous three categories.

APPENDIX

EASY REFERENCE TABLE

BUBBLE RADIUS, a (μm)	RES. FREQ (kHz)	DAMPING CONSTANT	$\frac{p^+}{p_1 p_2}$ $\frac{1}{Pa}$	TIME TO RISE 1"(SEC)
100	31.4	0.075	4.3×10^{-8}	1.44
70	44.6	0.085	2.7×10^{-8}	2.55
50	62.1	0.095	1.74×10^{-8}	4.61
40	77.3	0.100	1.34×10^{-8}	6.95
30	102.6	0.115	8.79×10^{-9}	12.0
20	152.9	0.13	5.25×10^{-9}	26.50
10	303.8	0.16	2.16×10^{-9}	105
9	337.7	0.16	1.94×10^{-9}	129
8	380.4	0.16	1.72×10^{-9}	163
7	435.8	0.16	1.50×10^{-9}	213
6	510.8	0.16	1.28×10^{-9}	--
5	618.0	0.16	1.05×10^{-9}	416

EXCITER		CARRIER		RECEIVER	
FREQ (kHz)	P_{PEAK} (Pa)	V_{pp}	P_{PEAK} (Pa)	FREQ (MHz)	M (V/Pa)
50	115	0.052	707	2.25	0.0000982
100	261	0.165	2242	2.3	0.0000969
150	244	0.41	5570.0	2.35	0.0000955
200	370	0.55	7472.0	2.4	0.0000951
250	515	0.94	12800.	2.45	0.0000939
300	980	1.10	14940.	2.5	0.0000936
350	1000	1.40	18250.	2.55	0.0000932
400	1190	1.98	26820.	2.6	0.0000934
		2.08	28260.	2.65	0.0000932
		2.55	34640.	2.7	0.0000937
		3.90	51800.	2.75	0.0000948
		4.0	47080.	2.8	0.0000947
		4.05	55020.	2.85	0.0000967
		5.0	66580.	2.9	0.0000966
		5.2	70650.	2.95	0.0000982
		6.0	81540.	3.0	0.0000974
		7.0	88080.	3.05	0.0000972
		7.67	102400.	3.1	0.0000966
		8.0	105300.		
		8.2	111400.		
		9.0	115300.		
		10.0	133200.		
		10.35	140600.		
		11.0	148900.		
		12.9	175300.		

REFERENCES

1. Newhouse, V. L. and Shankar, P. M., "Bubble Size Measurements Using the Nonlinear Mixing of Two Frequencies", Journal of the Acoustical Society of America (JASA), Vol. 75(5), pp. 1473-1477, May 1984.

2. Hampton, S. W., An Acoustic Bubble Density Measurement Technique for Surface Ship Wakes, Master's Thesis, Naval Postgraduate School, Monterey, California, September 1987.

3. Clay, S. C. and Medwin, H., Acoustical Oceanography: Principles and Applications, Wiley, 1977.

4. Beyer, R. T., Nonlinear Acoustics, Chapter Nine, Naval Sea Systems Command Contract N00024-72-C-1397, 1974.

5. Crum, L. A., "Acoustic Cavitation Series: Part Five, Rectified Diffusion", Ultrasoncis, pp. 215-223, September 1984.

6. Technical Report for Office of Naval Research, Contract N00014-84-C-0193, Mie Scattering as a Technique for the Sizing of Air Bubbles, by G. M. Hansen and L. A. Crum, pp. 5-7, 1 June 1983.

7. Kinsler, L. E., Frey, A. R., Coppens, A. B., and Sanders, J. V., Fundamentals of Acoustics, pp. 389-391, 3rd Edition, Wiley, 1982.

8. Bobber, R. J., Underwater Electroacoustic Measurements, pp. 17-36, Naval Research Laboratory, Washington, D. C., 1970.

9. Wilson, O. B., An Introduction to the Theory and Design of Sonar Transducers, p. 14, Peninsula Publishing, Los Altos, California, 1988.

10. Bruce, R. L. and Middleton, R. D., An Investiation of Acoustic Cavitation Produced By Pulsed Ultrasound, Master's Thesis, Naval Postgraduate School, Monterey, California, December 1987.

11. Baker, S. R., Analysis of Conventional Identical Transducer Reciprocity Calibration and Application to Plane-Wave Calibration, Naval Postgraduate School, Monterey, California, 20 September 1988.

INITIAL DISTRIBUTION LIST

		No. Copies
1.	Defense Technical Information Center Cameron Station Alexandria, Virginia 22304-6145	2
2.	Library, Code 0142 Naval Postgraduate School Monterey, California 93943-5002	2
3.	Professor Anthony A. Atchley, Code 61Ay Physics Department Naval Postgraduate School Monterey, California 93943-5002	5
4.	Professor S. L. Garrett, Code 61Gx Physics Department Naval Postgraduate School Monterey, California 93943-5002	1
5.	Professor Herman Medwin, Code 61Md Physics Department Naval Postgraduate School Monterey, California 93943-5002	1
6.	Dr. L. E. Hargrove Physics Division, Code 1112 Office of Naval Research 800 N. Quincy Street Arlington, Virginia 22217	1
7.	Dr. Larry Crum National Center for Physical Acoustics University, Mississippi 38677	1
8.	Commander, Naval Coastal Systems Center Dr. Elan Moritz, Code 2230 Panama City, Florida 32407-5000	2
9.	Commander, Naval Coastal Systems Center Dr. Kerry Commander, Code 2120 Panama City, Florida 32407-5000	2

10. Commander, Naval Coastal Systems Center 2
Clifton Bonney, Code 3210
Panama City, Florida 32407-5000

11. Lieutenant Ernest R. Lineberger, USN 2
Department Head School Class 107
Surface Warfare Officers School Command
Newport, Rhode Island 02841-5012

END

FILMED

6-89

DTIC

SUPPLEMENTARY

INFORMATION

AD-A207286

23 August 1989

ERRATA for thesis submitted by Ernest R. Lineberger, III, December 1988
Naval Postgraduate School, Monterey, Ca.

"Bubble Detection Using a Dual Frequency Sound Field"

Page 3	Fifth line from bottom: "P_A" should be "p_A" as in equation (1)
Page 3	Second line from bottom: "!" should appear between "bubble" and "taken"
Page 12	Eleventh line from top: "20" should be "30"
Page 13	Second line from top: "as" should be "is"
Page 23	Table 5 Title: "C_1/C_o" should be "C_i/C_o" as in equation (3)
Page 46	Sixth line from bottom: Sentence ends between "T" and "second" should be "T. Second,"
Page 46	Second line from bottom: Sentence ends at "R", should be "R. The"
Page 50	Equation (16) Numerator "P_F^2" should be "p_F^2" (i.e. lower case, p) Denominator "ρ" missing, should be "$\rho_o C$"
Page 60	Fourth line from top: "and" should be "an"
Page 61	Equation (27) Numerator should be "2A" not "2λd"
Page 67	Figure 14 precedes introduction on page 68 (chg 67 to 68 and 68 to 67)
Page 109	Tenth line from top: "semed" should be "seemed"